

# Universal competitive spectral scaling from the critical non-Hermitian skin effect

Fang Qin,<sup>1,\*</sup> Ye Ma,<sup>1</sup> Ruizhe Shen,<sup>1</sup> and Ching Hua Lee<sup>1,†</sup>

<sup>1</sup>*Department of Physics, National University of Singapore, Singapore 117551, Singapore*

(Dated: April 27, 2023)

Recently, it was discovered that certain non-Hermitian systems can exhibit qualitative different properties at different system sizes, such as being gapless at small sizes and having topological edge modes at large sizes  $L$ . This dramatic system size sensitivity is known as the critical non-Hermitian skin effect (cNHSE), and occurs due to the competition between two or more non-Hermitian pumping channels. In this work, we rigorously develop the notion of a size-dependent generalized Brillouin zone (GBZ) in a general multi-component cNHSE model ansatz, and found that the GBZ exhibits a universal  $a + b^{1/(L+1)}$  scaling behavior. In particular, we provided analytical estimates of the scaling rate  $b$  in terms of model parameters, and demonstrated their good empirical fit with two paradigmatic models, the coupled Hatano-Nelson model with offset, and the topologically coupled chain model with offset. We also provided analytic result for the critical size  $L_c$ , below which cNHSE scaling is frozen. The cNHSE represents the result of juxtaposing different channels for bulk-boundary correspondence breaking, and can be readily demonstrated in non-Hermitian metamaterials and circuit arrays.

## I. INTRODUCTION

Non-Hermitian systems harbor a host of interesting physics not found in equilibrium systems, such as exceptional point sensitivity and robustness [1–17], enlarged symmetry classes [18–21], and intrinsically non-equilibrium topological phases [22–35]. Once thought to exist almost exclusively as mathematical constructs, these novel phenomena have one by one been experimentally demonstrated in the recent years, thanks to rapid technical advances in ultracold atomic gases [36–40], electrical circuits [41–53], photonic systems [11, 23, 54–62], coupled acoustic cavities [63–67], as well as other metamaterials [68–80].

A particularly intriguing type of non-Hermitian phenomenon is the breaking of conventional bulk-boundary correspondences (BBCs), which generically occurs whenever reciprocity is also broken. Topological BBCs relate boundary topological states with bulk topological invariants, and are cherished tenets in topological classification [81–86]. The most well-studied type of non-Hermitian BBC is the non-Hermitian skin effect (NHSE) [87–104], which is characterized by exponentially large boundary state accumulation that leads to very different energy spectra under open and periodic boundary conditions (OBCs and PBCs). To restore an effective bulk theory, the customary approach has been to define a generalized Brillouin zone (GBZ) with complexified momentum [91, 105–112], such that quantities computed in the GBZ correctly correspond to physical observations.

Most interesting is the relatively little-understood scenario of *critical* NHSE (cNHSE) [113], where even the scaling properties of the system are drastically modified by non-Hermiticity. For instance, the same metamaterial

exhibiting cNHSE can behave qualitatively differently at different system sizes, such as being gapless (metallic) at small sizes but topologically insulating at large sizes [113–116]. Physically, such peculiar size-dependent transitions are due to the competition between multiple NHSE channels (non-reciprocity strengths) in the system – at different length scales, the same physical coupling can be “renormalized” to very different values dependent on the dominant NHSE channel. Due to their peculiar size dependency, the cNHSE systems also harbor different entanglement scaling laws [113] from those of other Hermitian and non-Hermitian phases [7–9, 117–126].

In this work, we focus on addressing the following open question: How exactly can we understand cNHSE scaling behavior in terms of the GBZ, which is widely used for restoring the BBC in the thermodynamic limit? Specifically, we find that a cNHSE system of finite size can be accurately described through an “interpolated” GBZ that lies between the competing GBZs describing the same (but behaviorally distinct) system in the small and large size limits. Furthermore, this interpolation occurs at a rate obeying a universal exponential scaling law, with exponent inversely proportional to system size. Since the effective GBZ allows one to represent the system with a Hamiltonian with an effective Bloch description, this scaling law carries over into most physical properties of cNHSE lattices.

To motivate and substantiate our results, we consider a generic two-component ansatz for modeling a cNHSE system with two competing NHSE channels. Our ansatz encompasses the minimal model studied in Ref. [127], and showcases how some of its results can be generalized in the context of arbitrary NHSE channels. By subsequently specializing into two paradigmatic models, we provide detailed derivations of the universal  $a + b^{1/(L+1)}$  scaling behavior governing the effective finite-size GBZ, where  $L$  is the system size, and  $a, b$  constants depending on the model details. We also provide detailed and empirically verified estimates of the lower critical system

\* qinfang@nus.edu.sg

† phylch@nus.edu.sg

size  $L_c$  above which such a scaling relation holds.

We pause to briefly elaborate on the experimental prospects for the cNHSE models discussed in this work. Most directly, electrical circuits, i.e., “topoelectrical circuits” can be connected in very versatile manners, and are thus readily suited for their experimental implementation [41–53]. In general, operation amplifiers serve as almost perfectly linear components with asymmetric Laplacians [42], and are thus ideal building blocks for models with the asymmetric couplings necessary for cNHSE. Recently the coupled Hatano-Nelson cNHSE model of this work has also been realized in an even simpler experimental circuit platform [52] involving only RLC circuit components, since asymmetric couplings can be rendered symmetric via a basis rotation in this model. Circuit realizations can also be largely generalized to photonic platforms [55, 128–134]. Coupled resonator arrays can be used to experimentally realize the arrays in our models, with the ring resonators [128] (which are the primary resonators) representing the sites in our model chains. Experimental values of the hoppings in such photonic systems are highly tunable, ranging approximately from 5 GHz to 30 GHz [135, 136]. The optical gain and loss in a photonic system can be used to experimentally realize the gain and loss in our non-Hermitian models.

The paper is organized as follows: In section II, we set up the cNHSE formalism using a general two-component ansatz. Next, we illustrate our results through detailed calculations on two paradigmatic models, a coupled Hatano-Nelson model with energy offset (section III) and a model with size-dependent topology (section IV). We show how their OBC spectra and effective GBZs depend greatly on the system size, and provide quantitative derivations of their exponential scale dependence, as well as the critical system size above which such scaling holds. In section V, we demonstrate the robustness of the scaling of imaginary energy against substantial disorder. Finally, we summarize the key findings in the discussion in section VI.

## II. GENERAL TWO-COMPONENT CNHSE ANSATZ

To understand the cNHSE phenomenon, we first review the concept of the GBZ. The GBZ formalism restores the BBC via a complex momentum deformation. For a momentum-space one-dimensional (1D) Hamiltonian  $H(z)$  with  $z = e^{ik}$ , the GBZ corresponding to an eigenenergy  $E$  can be obtained from solving for  $z = e^{ik}$  in the following characteristic Laurent polynomial [89, 105]:

$$f(z, E) := \det[H(z) - E \mathbb{I}] = 0. \quad (1)$$

For  $E$  that does not coincide with any of the PBC eigenenergies, i.e., eigenvalues of  $H(e^{ik})$  for real  $k$ , we must have complex  $k = -i \ln z$ . Such  $E$  lies in the OBC spectrum when the latter is very different from the PBC spectrum. It can be shown that [87, 89, 91, 99, 101, 110]

in the thermodynamic limit, the OBC eigenenergies are given by [137] solutions of  $k$  that are doubly degenerate in both  $\text{Im}(k)$  and  $E$ : For such solutions, we define the GBZ as  $\kappa(k)$ , where the complex momentum deformation is given by  $k \rightarrow k + i\kappa(k)$ . In other words, we say that the conventional (Bloch) BZ is replaced by the (non-Bloch) GBZ defined by  $z \rightarrow e^{ik} e^{-\kappa(k)}$ .

To understand how the GBZ formalism needs to be modified in a cNHSE system, we start from a generic two-component ansatz cNHSE Hamiltonian, written in the component basis  $C_{\mathbf{k}} = (c_{\mathbf{k},A}, c_{\mathbf{k},B})^T$  as

$$\mathcal{H}_g(z) = \begin{pmatrix} \mathcal{H}^{aa}(z) & \mathcal{H}^{ab}(z) \\ \mathcal{H}^{ba}(z) & \mathcal{H}^{bb}(z) \end{pmatrix} = \sum_{n=-n_-}^{n_+} \begin{pmatrix} h_n^{aa} & h_n^{ab} \\ h_n^{ba} & h_n^{bb} \end{pmatrix} z^n, \quad (2)$$

where  $n_{\pm} \in \mathbb{Z}$ ,  $z = e^{ik}$ . In principle, cNHSE exists as long as  $\mathcal{H}^{aa}$  and  $\mathcal{H}^{bb}$  exhibit dissimilar inverse skin localization lengths  $\kappa(k)$ , and couplings  $\mathcal{H}^{ab}, \mathcal{H}^{ba} \neq 0$ . The former condition is equivalent to having asymmetric hoppings  $h_n^{aa} \neq h_{-n}^{aa}$  and  $h_n^{bb} \neq h_{-n}^{bb}$  for some  $n$ , as well as  $h_n^{aa}/h_{-n}^{aa} \neq h_n^{bb}/h_{-n}^{bb}$ .

To implement OBCs, we first Fourier transform to real space, where one obtains the real-space tight-binding Hamiltonian

$$H_{gr} = \sum_{i=1}^L \sum_{n=-n_-}^{n_+} C_i^\dagger \begin{pmatrix} h_n^{aa} & h_n^{ab} \\ h_n^{ba} & h_n^{bb} \end{pmatrix} C_{i+n}, \quad (3)$$

where  $L$  is the system size, i.e., number of unit cells,  $1 \leq n_{\pm} \leq L/2$ ,  $C_i = (c_{i,A}, c_{i,B})^T$  with the annihilation (creation) operator  $c_{i,\alpha}$  ( $c_{i,\alpha}^\dagger$ ) on site  $\alpha$  ( $\alpha = A, B$ ) in cell  $i$ . For a real-space wave function  $|\psi\rangle = (\psi_{1,A}, \psi_{1,B}, \psi_{2,A}, \psi_{2,B}, \dots, \psi_{L,A}, \psi_{L,B})^T$ , we express the real-space Schrödinger equation  $\mathcal{H}_{gr}|\psi\rangle = E_{\text{OBC}}|\psi\rangle$  as

$$\begin{cases} \sum_{n=-n_-}^{n_+} (h_n^{aa} \psi_{i+n,A} + h_n^{ab} \psi_{i+n,B}) = E_{\text{OBC}} \psi_{i,A}, \\ \sum_{n=-n_-}^{n_+} (h_n^{ba} \psi_{i+n,A} + h_n^{bb} \psi_{i+n,B}) = E_{\text{OBC}} \psi_{i,B}, \end{cases} \quad (4)$$

where  $\mathcal{H}_{gr}$  is the Hamiltonian matrix of  $H_{gr}$  in the basis  $(C_1, C_2, \dots, C_L)^T$  and  $E_{\text{OBC}}$  is the eigenenergy under OBC. To relate to the complex momenta present in non-Hermitian skin modes, we solve the real-space Schrödinger equation via the ansatz

$$(\psi_{n,A}, \psi_{n,B})^T = \sum_j (\beta_j)^n \begin{pmatrix} \phi_A^{(j)} \\ \phi_B^{(j)} \end{pmatrix}, \quad (5)$$

where  $A, B$  are the site indices in the cell, and  $n$  represents the position of the cell (A,B) in the real space. Here,  $\beta_j$  are specific solutions to  $z = e^{ik}$ , and characterizes the spatial localization of the boundary skin-localized wave function. By substituting Eq. (5) into (4), we can write

the bulk eigenequation as

$$\begin{cases} \left[ \sum_{n=-n_-}^{n_+} h_n^{aa}(\beta_j)^n - E_{\text{OBC}} \right] \phi_A^{(j)} + \sum_{n=-n_-}^{n_+} h_n^{ab}(\beta_j)^n \phi_B^{(j)} = 0, \\ \sum_{n=-n_-}^{n_+} h_n^{ba}(\beta_j)^n \phi_A^{(j)} + \left[ \sum_{n=-n_-}^{n_+} h_n^{bb}(\beta_j)^n - E_{\text{OBC}} \right] \phi_B^{(j)} = 0. \end{cases} \quad (6)$$

Equation (6) can be recast into the energy dispersion characteristic equation

$$\begin{aligned} E_{\text{OBC}}^2 - \sum_{n=-n_-}^{n_+} (h_n^{aa} + h_n^{bb}) (\beta_j)^n E_{\text{OBC}} \\ + \left[ \sum_{n=-n_-}^{n_+} h_n^{aa}(\beta_j)^n \right] \left[ \sum_{n=-n_-}^{n_+} h_n^{bb}(\beta_j)^n \right] \\ - \left[ \sum_{n=-n_-}^{n_+} h_n^{ab}(\beta_j)^n \right] \left[ \sum_{n=-n_-}^{n_+} h_n^{ba}(\beta_j)^n \right] = 0, \quad (7) \end{aligned}$$

By eliminating  $\phi_B^{(j)}$  in terms of  $\phi_A^{(j)}$ , we obtain  $2M$  simultaneous linear equations in  $\phi_A^{(j)}$ , ( $j = 1, 2, \dots, 2M$ ), which yield nonvanishing solutions only if the determinant

$$\begin{vmatrix} F_1^{(a,1)} \beta_1 & F_2^{(a,1)} \beta_2 & \cdots & F_{2M}^{(a,1)} \beta_{2M} \\ F_1^{(b,1)} \beta_1 & F_2^{(b,1)} \beta_2 & \cdots & F_{2M}^{(b,1)} \beta_{2M} \\ \vdots & \vdots & \vdots & \vdots \\ F_1^{(a,n_+)} (\beta_1)^{n_+} & F_2^{(a,n_+)} (\beta_2)^{n_+} & \cdots & F_{2M}^{(a,n_+)} (\beta_{2M})^{n_+} \\ F_1^{(b,n_+)} (\beta_1)^{n_+} & F_2^{(b,n_+)} (\beta_2)^{n_+} & \cdots & F_{2M}^{(b,n_+)} (\beta_{2M})^{n_+} \\ G_1^{(a,1)} (\beta_1)^{L-(n_--1)} & G_2^{(a,1)} (\beta_2)^{L-(n_--1)} & \cdots & G_{2M}^{(a,1)} (\beta_{2M})^{L-(n_--1)} \\ G_1^{(b,1)} (\beta_1)^{L-(n_--1)} & G_2^{(b,1)} (\beta_2)^{L-(n_--1)} & \cdots & G_{2M}^{(b,1)} (\beta_{2M})^{L-(n_--1)} \\ \vdots & \vdots & \vdots & \vdots \\ G_1^{(a,n_-)} (\beta_1)^L & G_2^{(a,n_-)} (\beta_2)^L & \cdots & G_{2M}^{(a,n_-)} (\beta_{2M})^L \\ G_1^{(b,n_-)} (\beta_1)^L & G_2^{(b,n_-)} (\beta_2)^L & \cdots & G_{2M}^{(b,n_-)} (\beta_{2M})^L \end{vmatrix} = 0, \quad (8)$$

as derived in more detail in Appendix A. This determinant expression captures the constraints from OBCs at both boundaries. In general, it is a complicated expression, but can still be written explicitly in terms of  $\beta_j$  and  $E_{\text{OBC}}$  for the two-band ansatz:

$$F_j^{(a,i)} = \sum_{n=-(i-1)}^{n_+} (h_n^{aa} + f_j h_n^{ab}) (\beta_j)^n - E_{\text{OBC}}, \quad (9)$$

$$F_j^{(b,i)} = \sum_{n=-(i-1)}^{n_+} (h_n^{ba} + f_j h_n^{bb}) (\beta_j)^n - f_j E_{\text{OBC}}, \quad (10)$$

$$G_j^{(a,i)} = \sum_{n=-n_-}^{n_--i} (h_n^{aa} + f_j h_n^{ab}) (\beta_j)^n - E_{\text{OBC}}, \quad (11)$$

$$G_j^{(b,i)} = \sum_{n=-n_-}^{n_--i} (h_n^{ba} + f_j h_n^{bb}) (\beta_j)^n - f_j E_{\text{OBC}}, \quad (12)$$

where we have labeled the solutions  $\beta_j$  with increasing magnitude  $|\beta_1| \leq |\beta_2| \leq \cdots \leq |\beta_{2M}|$ . Here  $M = n_- + n_+$ .

Importantly, the key property required for restoring BBCs – the complex momentum deformation (effective GBZ) – does not require intimate knowledge of most of these  $\beta$  solutions. This is because fundamentally, the required complex deformation depends on the decay rate of the eigenstates, which turns out to depend only on two dominant  $\beta$  solutions. Below, we derive the precise conditions from the bulk eigenequations (6) as well as constraints from the OBCs  $\psi_{-n_-, \alpha} = \cdots = \psi_{-1, \alpha} = \psi_{0, \alpha} = \psi_{L+1, \alpha} = \psi_{L+2, \alpha} = \cdots = \psi_{L+n_+, \alpha} = 0$  ( $\alpha = A, B$ ;  $1 \leq n_{\pm} \leq L/2$ ).

where

$$\begin{aligned} f_j &= \frac{\phi_B^{(j)}}{\phi_A^{(j)}} = \frac{E_{\text{OBC}} - \sum_{n=-n_-}^{n_+} h_n^{aa} (\beta_j)^n}{\sum_{n=-n_-}^{n_+} h_n^{ab} (\beta_j)^n} \\ &= \frac{\sum_{n=-n_-}^{n_+} h_n^{ba} (\beta_j)^n}{E_{\text{OBC}} - \sum_{n=-n_-}^{n_+} h_n^{bb} (\beta_j)^n}. \end{aligned} \quad (13)$$

Equation (8) can be rearranged in a compact multivariate polynomial form

$$\sum_{P, Q} J(\beta_{i \in P}, \beta_{j \in Q}, E_{\text{OBC}}) \left[ \prod_{i \in P} (\beta_i)^k \right] \left[ \prod_{j \in Q} (\beta_j)^{k'} \right] = 0, \quad (14)$$

where  $k = 1, \dots, n_+$ ,  $k' = L - (n_- - 1), \dots, L$ , sets  $P$  and  $Q$  are two disjoint subsets of the set  $\{1, 2, \dots, 2M\}$  with  $M$  elements, respectively, and  $J(\beta_{i \in P}, \beta_{j \in Q}, E_{\text{OBC}})$  is the

$E_{\text{OBC}}$ -dependent coefficient corresponding to a particular permutation of  $P$  and  $Q$ . By separating the product contributions of the  $\beta$ s which are exponentiated by  $L$ , we can extract out contributions that scale differently with  $L$ .

Furthermore, in the case  $n_+ = n_-$  where the maximal left and right hopping distances are the same, Eq. (14) simplifies to

$$\sum_{P,Q} J(\beta_{i \in P}, \beta_{j \in Q}, E_{\text{OBC}}) \left[ \prod_{i \in P} (\beta_i)^{L+1} \right] = 0. \quad (15)$$

In the thermodynamic limit, the large  $L$  in the exponents picks up the slowest decaying terms, and these would be the physically dominant contributions amidst the complicated jungle of terms. Specifically, in Eq. (15), we find that there are two leading terms proportional to  $(\beta_M \beta_{M+2} \beta_{M+3} \cdots \beta_{2M})^{L+1}$  and  $(\beta_{M+1} \beta_{M+2} \beta_{M+3} \cdots \beta_{2M})^{L+1}$ , which yield in the limit of large system size  $L$

$$\left| \frac{\beta_M}{\beta_{M+1}} \right| \simeq \left| - \frac{J(\beta_{i \in P_1}, \beta_{j \in Q_1}, E_{\text{OBC}})}{J(\beta_{i \in P_2}, \beta_{j \in Q_2}, E_{\text{OBC}})} \right|_{E_{\text{OBC}}=E_\infty}^{\frac{1}{L+1}}, \quad (16)$$

where  $P_1 = \{M+1, M+2, M+3, \dots, 2M\}$ ,  $Q_1 = \{1, 2, 3, \dots, M\}$ ,  $P_2 = \{M, M+2, M+3, \dots, 2M\}$ ,  $Q_2 = \{1, 2, \dots, M-2, M-1, M+1\}$ ,  $M = n_+ + n_-$ , and  $L$  is the system size with  $L \rightarrow \infty$ . We emphasize that the form of this result Eq. (16) with  $L \rightarrow \infty$  still holds for general higher-component or multi-band models [see Eq. (B19), albeit with more complicated  $J$  functions], as derived in Appendix B. The details are complicated, but physically, we expect qualitatively similar behavior because the critical NHSE essentially arises from the competition between the NHSE and the couplings, and with greater number of bands, we will have more avenues for the competition. But unless the model is fine tuned, we will generically still see the direct competition between pairs of bands, which thus reduces qualitatively to two-band behavior.

We comment on a few key takeaways from Eq. (16). Without any assumption on the detailed hoppings in the 1D tight-binding model, we showed how the requirement of satisfying OBCs at both ends generically lead to Eq. (16), which relates  $|\beta_M/\beta_{M+1}|^{L+1}$  with a combination of  $L$ -independent model parameters. It picks out the solutions  $\beta_M$  and  $\beta_{M+1}$  of Eq. (7) as the dominant ones at large  $L$ , although in this regime, the  $L$  dependence is also generally weak since the exponent  $1/(L+1)$  changes slowly. Below, we discuss further on the large  $L$  and moderate  $L$  regimes separately.

In the thermodynamic limit of  $L \rightarrow \infty$ , the right hand side of Eq. (16) tends to unity, giving rise to the standard GBZ result  $|\beta_M| = |\beta_{M+1}|$  discussed in [87, 89, 91, 110, 113, 127, 138]. Hence, to draw the GBZ for  $L \rightarrow \infty$ , we uniformly vary the relative phase between  $\beta_M$  and  $\beta_{M+1}$ , and trace out the trajectory  $\mathcal{C}_\beta$  satisfying  $|\beta_M| = |\beta_{M+1}|$ . Since  $L$  is large, each point in the GBZ curve is separated

by a  $2\pi/L$  phase interval that converges to a continuum, resulting in continuum complex energy bands.

For finite  $L$  away from the thermodynamic limit, we emphasize that this standard GBZ construction for  $E_\infty = \lim_{L \rightarrow \infty} E_{\text{OBC}}$  may no longer be valid. While in many cases,  $E_{\text{OBC}}$  does not change significantly as  $L$  is extrapolated down to moderate [i.e.,  $L \sim \mathcal{O}(10)$ ], in cNHSE cases, the spectra and hence other physical properties vary strongly with system size. To characterize such cNHSE scenarios at finite  $L$ , we note from Eq. (16) that the magnitudes  $|\beta_M|$  and  $|\beta_{M+1}|$  can no longer be treated as equal. Physically, this implies that the OBC eigenstates are superpositions of different modes with inverse spatial decay lengths of either  $-\ln|\beta_M|$  or  $-\ln|\beta_{M+1}|$ . As such, the effective cNHSE GBZ is described by *both*  $|\beta_M|$  and  $|\beta_{M+1}|$ , which are no longer equal. Contributions from other  $\beta_j$  solutions affect the eigenstate decay rates negligibly even in the presence of cNHSE, as numerically verified for our illustrative coupled Hatano-Nelson model in Appendix C.

In the following two sections, we shall elaborate on how the pair of GBZ solutions  $|\beta_M|$  and  $|\beta_{M+1}|$  scale with system size  $L$ . Since the exact scaling dependencies can be highly complicated, we shall illustrate our results concretely through two paradigmatic cNHSE models, the minimal coupled Hatano-Nelson model with energy offset in section III and a model with size-dependent topological states in section IV.

### III. COUPLED HATANO-NELSON MODEL WITH ENERGY OFFSET

In this section, we elaborate on a cNHSE model formed by coupling the simplest possible NHSE chains – two equal and oppositely oriented Hatano-Nelson chains. Going beyond the minimal model introduced in Ref. [127], which provided elegant analytic results, we additionally introduce on-site energy offsets  $\pm V$  on the two chains, respectively, such that the inter-chain coupling now also faces nontrivial competition from the energetic separation of  $2|V|$ . The coupled chains are illustrated in Fig. 1(a), with each chain constituting one of the sublattices  $A$  and  $B$ . In the basis  $C_{\mathbf{k}} = (c_{\mathbf{k},A}, c_{\mathbf{k},B})^T$ , its momentum-space Hamiltonian is

$$\mathcal{H}(z) = \begin{pmatrix} t_a^+ z + t_a^-/z + V & t_0 \\ t_0 & t_b^+ z + t_b^-/z - V \end{pmatrix}, \quad (17)$$

where  $t_a^\pm = t_1 \pm \delta_a$ ,  $t_b^\pm = t_1 \pm \delta_b$ ,  $t_0$  is the inter-chain hopping, and  $\pm V$  is the on-site potential energy. We denote  $z = e^{ik}$  as before, where  $k$  is the momentum. It is related via Fourier transformation to the corresponding

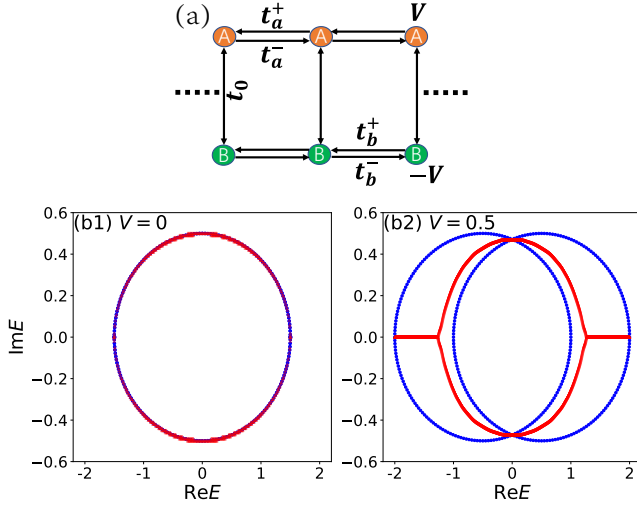


FIG. 1. (a) Coupled Hatano-Nelson chain model [Eq. (18)] with inter-chain hopping  $t_0$ , intra-chain hopping asymmetries  $t_a^\pm = t_1 \pm \delta_a$  and  $t_b^\pm = t_1 \pm \delta_b$ , and chain energy offsets  $\pm V$ . (b) Energy spectra of Eq. (18) under PBCs (blue) and OBC (red) in the  $L \rightarrow \infty$  limit for (b1)  $V = 0$  and (b2)  $V = 0.5$ . Parameters are  $t_0 = 0.01$ ,  $t_1 = 0.75$ , and  $\delta_a = -\delta_b = 0.25$ . While the PBC and OBC spectra coincide in the  $V = 0$  case studied in [127], they deviate when  $V \neq 0$ , leading to broken bulk-boundary correspondence.

real-space tight-binding Hamiltonian

$$H_r = \sum_n \left( t_a^+ c_{n,A}^\dagger c_{n+1,A} + t_a^- c_{n+1,A}^\dagger c_{n,A} + t_0 c_{n,A}^\dagger c_{n,B} + t_b^+ c_{n,B}^\dagger c_{n+1,B} + t_b^- c_{n+1,B}^\dagger c_{n,B} + t_0 c_{n,B}^\dagger c_{n,A} + V c_{n,A}^\dagger c_{n,A} - V c_{n,B}^\dagger c_{n,B} \right), \quad (18)$$

where  $c_{n,\alpha}$  ( $c_{n,\alpha}^\dagger$ ) is the annihilation (creation) operator on site  $\alpha$  ( $\alpha = A, B$ ) in unit cell  $n$ . Evidently,  $t_a^+/t_a^-$  and  $t_b^+/t_b^-$  are the hopping asymmetries of chains A and B.

The energy eigenvalues of the Hamiltonian (17) under PBCs are given by

$$E_{\text{PBC}}^{(\pm)}(k) = 2t_1 \cos k + i(\delta_a + \delta_b) \sin k \pm \sqrt{[i(\delta_a - \delta_b) \sin k + V]^2 + t_0^2}, \quad (19)$$

where  $k \in \mathbb{R}$  and  $t_a^\pm = t_1 \pm \delta_a$ ,  $t_b^\pm = t_1 \pm \delta_b$ . In Fig. 1(b1), we see that in the large- $L$  limit, the PBC spectrum (blue) agrees well with the OBC spectrum (red) only in the  $V = 0$  case which Ref. [127] has considered. When  $V \neq 0$  [Fig. 1(b2)], the OBC spectrum lies in the interior of the PBC loops and can only agree with  $E_{\text{PBC}}^{(\pm)}(k)$  if we perform an appropriate complex momentum deformation  $k \rightarrow k + i\kappa(k)$  [89, 91, 99, 101, 110, 113]. While it may appear here that the  $V = 0$  case does not experience BBC breaking (i.e., the NHSE), that is actually untrue once we consider finite system sizes [127]. Below, we show that this model exhibits cNHSE at finite system sizes for *all*

values of  $V$ , and compare some analytic approximations with numerical results.

### A. Finite-size scaling from the cNHSE

To understand how the PBC and OBC spectra differ beyond the thermodynamic limit shown in Figs. 1(b1) and 1(b2), we examine the real-space Schrödinger's equation  $\mathcal{H}_r|\psi\rangle = E_{\text{OBC}}|\psi\rangle$ , where  $|\psi\rangle = (\psi_{1,A}, \psi_{1,B}, \psi_{2,A}, \psi_{2,B}, \dots, \psi_{n,A}, \psi_{n,B}, \dots)^T$ :

$$\begin{cases} t_a^- \psi_{n-1,A} + t_0 \psi_{n,B} + t_a^+ \psi_{n+1,A} + V \psi_{n,A} = E_{\text{OBC}} \psi_{n,A}, \\ t_b^- \psi_{n-1,B} + t_0 \psi_{n,A} + t_b^+ \psi_{n+1,B} - V \psi_{n,B} = E_{\text{OBC}} \psi_{n,B}, \end{cases} \quad (20)$$

where  $\mathcal{H}_r$  is the Hamiltonian matrix of  $H_r$  in the basis  $(C_1, C_2, \dots, C_j, \dots)^T$ . Based on the approach developed in the section II, we can use as an eigenstate ansatz which is a linear combination of  $\beta$  solutions, such as to solve the real-space Schrödinger equation [87, 112, 127]:

$$\begin{pmatrix} \psi_{n,A} \\ \psi_{n,B} \end{pmatrix} = \sum_{j=1}^4 (\beta_j)^n \begin{pmatrix} \phi_A^{(j)} \\ \phi_B^{(j)} \end{pmatrix}. \quad (21)$$

This allows us to rewrite Eq. (20) as

$$\begin{pmatrix} t_a^+ \beta + t_a^- \beta^{-1} + V & t_0 \\ t_0 & t_b^+ \beta + t_b^- \beta^{-1} - V \end{pmatrix} \begin{pmatrix} \phi_A \\ \phi_B \end{pmatrix} = E_{\text{OBC}} \begin{pmatrix} \phi_A \\ \phi_B \end{pmatrix}, \quad (22)$$

where we have written  $\beta_j = \beta$  and  $\phi_\alpha^{(j)} = \phi_\alpha$  ( $\alpha = A, B$ ) for notational simplicity, since Eq. (22) applies separately to different  $j$ . Essentially, this ansatz has allowed us to replace  $z = e^{ik}$  by  $\beta$ . Nontrivial solutions to Eq. (22) satisfy the bulk characteristic dispersion equation

$$\begin{aligned} & t_a^+ t_b^+ \beta^2 - [(t_a^+ + t_b^+) E_{\text{OBC}} + (t_a^+ - t_b^+) V] \beta \\ & + (t_a^+ t_b^- + t_a^- t_b^+ + E_{\text{OBC}}^2 - t_0^2 - V^2) \\ & - [(t_a^- + t_b^-) E_{\text{OBC}} + (t_a^- - t_b^-) V] \beta^{-1} + t_a^- t_b^- \beta^{-2} = 0. \end{aligned} \quad (23)$$

For each value of  $E_{\text{OBC}}$ , there are four solutions  $\beta = \beta_j$ ,  $j = 1, 2, 3, 4$ , since the maximal and minimal powers of  $\beta$  are  $n_+ = n_- = 1$ .

#### 1. Finite-size scaling of the OBC spectra

To understand the OBC spectrum  $E_{\text{OBC}}$  in terms of non-Bloch theory, we need to obtain its effective GBZ. For finite  $L$ , the GBZ comprises the two dominant  $\beta$  solutions such that  $E_{\text{PBC}}(-i \log \beta)$  numerically coincides with  $E_{\text{OBC}}$ . The numerically computed  $E_{\text{OBC}}$  is shown in Fig. 2 for both (a)  $V = 0$  and (b)  $V = 0.5$ . Evidently, the OBC spectra in both cases depends strongly on  $L$ , being real for small  $L$  (i.e.,  $L = 10$ ), and gradually morphing into the large  $L$  spectrum previously shown



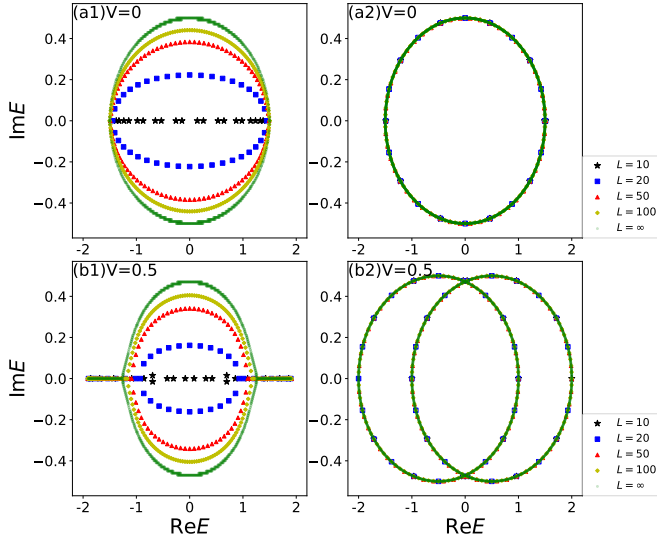


FIG. 2. OBC energy spectra of the coupled Hatano-Nelson model Hamiltonian (18) with (a1)  $V = 0$  and (b1)  $V = 0.5$  at different finite system sizes  $L = 10$  (black), 20 (blue), 50 (red), 100 (yellow),  $\infty$  (green). When  $V = 0$ , the spectrum is real for short chains, but complex for long chains due to the strong effective couplings from large  $L$ . But interestingly for  $V \neq 0$ , short chains can possess some complex energies, and long chains possess some real energies. PBC energy spectra of the coupled Hatano-Nelson model Hamiltonian (18) with (a2)  $V = 0$  and (b2)  $V = 0.5$  at different finite system sizes  $L = 10$  (black), 20 (blue), 50 (red), 100 (yellow),  $\infty$  (green). Parameters are  $t_0 = 0.01$ ,  $t_1 = 0.75$ , and  $\delta_a = -\delta_b = 0.25$ , the same as those in Fig. 1.

in Fig. 1. Physically, the spectrum remains real when the couplings (here with small bare values  $t_0 = 0.01$ ) are strong enough for the directed amplifications from both chains to cancel [139]; as the system gets larger, the cNHSE becomes exponentially stronger and the couplings serve to “close up” [52, 115, 140] the amplification loops, causing unchecked amplification that corresponds to complex energies. For  $V \neq 0$ , some eigenenergies can remain real even at arbitrarily large system sizes presumably because the potential offsets obstruct unchecked amplification.

## 2. From OBC spectra to size-dependent cNHSE GBZs

While the size-dependent spectra in Fig. 2 unambiguously signify the presence of cNHSE, size-dependencies in the spectra are model-specific. Key to more fundamental understanding of cNHSE scaling is the scaling behavior of the GBZ [141]. To compute the GBZ, we substitute the OBC energies into the characteristic equation (23) and obtain the  $\beta$  solutions. Here, for each  $E_{\text{OBC}}$  point, we have four solutions  $|\beta_1| \leq |\beta_2| \leq |\beta_3| \leq |\beta_4|$  and the GBZ is given by the two solutions  $\beta_M = \beta_2$  and  $\beta_{M+1} = \beta_3$ . Figure 3 shows the GBZ computed at various finite system sizes  $L = 10, 20, 50, 100$ ; the  $L = \infty$  case (green)

is plotted by solving Eq. (23) with the standard condition  $|\beta_2| = |\beta_3|$  (i.e., intersecting  $\beta_2$  and  $\beta_3$  solution curves) [91, 106–112] valid in the thermodynamic limit.

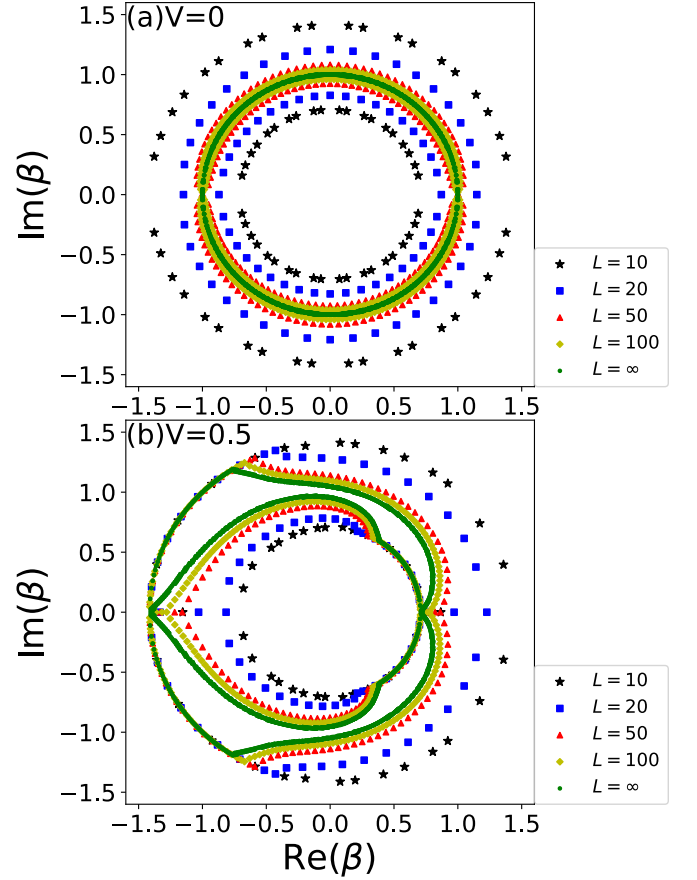


FIG. 3. GBZ of the coupled Hatano-Nelson model Hamiltonian (18) at different finite system sizes  $L = 10$  (black), 20 (blue), 50 (red), 100 (yellow),  $\infty$  (green) for (a)  $V = 0$  and (b)  $V = 0.5$ . At finite  $L$ , the GBZ is given by solutions  $\beta_M = \beta_2$  and  $\beta_{M+1} = \beta_3$ ; as  $L \rightarrow \infty$ , the  $\beta_2$  and  $\beta_3$  loops converge towards the standard GBZ solution  $|\beta_2| = |\beta_3|$ . Note that this standard GBZ can consist of two loops (as in (b)), since this is a two-band model. Parameters are  $t_0 = 0.01$ ,  $t_1 = 0.75$ , and  $\delta_a = -\delta_b = 0.25$ , the same as those in Fig. 1.

For the finite-size cases under  $V = 0$  shown in Fig. 3(a), there are two loops in the  $\text{Re}(\beta)$ - $\text{Im}(\beta)$  plane for each value of  $L$ , corresponding to the  $\beta_2$  and  $\beta_3$  solutions. As the system size  $L$  increases to infinity, they converge towards each other, as expected from the condition  $|\beta_2| = |\beta_3|$ . Similarly, for the  $V \neq 0$  case in Fig. 3(b), the two loops in the  $\text{Re}(\beta)$ - $\text{Im}(\beta)$  plane get closer and closer to each other as the system size  $L$  increases. However, in this case, they do not converge into one single loop because the GBZ solution  $|\beta_2| = |\beta_3|$  itself consists of two loops [green in Fig. 3(b)]. Here the GBZ solutions are also highly anisotropic in the wave number  $\arg(\beta)$ , exhibiting cusps at  $\beta$  corresponding to branch points in the spectrum [99, 101].

### 3. Finite scaling behavior of the GBZ

Having numerically seen how the GBZ varies with system size, we now rigorously derive the scaling rules governing it. To do so, we examine the OBC constraints in detail. As elaborated in Appendix D, imposing open boundaries at  $x = 1$  and  $x = L$ , i.e.,  $\psi_{0,\alpha} = \psi_{L+1,\alpha} = 0$  gives rise to the condition

$$\begin{aligned} & X_{1,4}X_{2,3} \left[ (\beta_1\beta_4)^{L+1} + (\beta_2\beta_3)^{L+1} \right] \\ & - X_{1,3}X_{2,4} \left[ (\beta_1\beta_3)^{L+1} + (\beta_2\beta_4)^{L+1} \right] \\ & + X_{1,2}X_{3,4} \left[ (\beta_1\beta_2)^{L+1} + (\beta_3\beta_4)^{L+1} \right] = 0, \end{aligned} \quad (24)$$

where  $X_{i,j}$  are defined as

$$X_{i,j} \equiv t_a^+(\beta_j - \beta_i) + t_a^-(\beta_j^{-1} - \beta_i^{-1}) \quad (25)$$

with  $i, j = 1, 2, 3, 4$ . This result is equivalent to Eq. (8), but specialized to our coupled Hatano-Nelson model Hamiltonian. Interestingly, it is independent of  $V$  and  $E_{\text{OBC}}$ , even though they both definitely affect the values of  $\beta_j$ , since the individual  $\beta_j$  solutions are determined by the characteristic dispersion equation (23). When  $L$  is varied, the  $\beta_j$  solutions of Eq. (23) vary since  $E_{\text{OBC}}$  changes with  $L$ . How exactly  $E_{\text{OBC}}$  can change is indirectly constrained by Eq. (24), which imposes a  $L$ -dependent relation between the  $\beta_j$  solutions corresponding to the value of  $E_{\text{OBC}}$ .

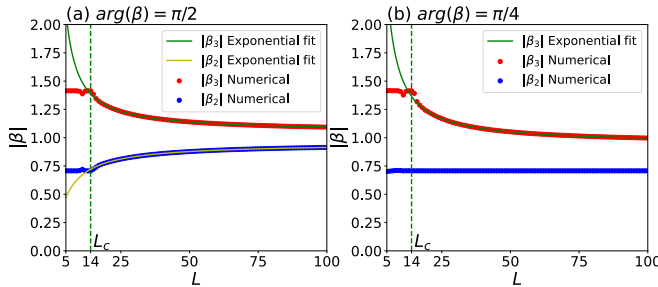


FIG. 4. The GBZ radii  $|\beta_2|$  and  $|\beta_3|$  of our coupled Hatano-Nelson model Hamiltonian (18) with  $V = 0.5$ , plotted against the system size  $L$  for (a)  $\arg(\beta) = \frac{\pi}{2}$  and (b)  $\arg(\beta) = \frac{\pi}{4}$ . Results obtained from the numerical OBC spectra exhibit excellent fitting with the exponential scaling of Eq. (28), with fitted parameters  $a(\arg(\beta) = \frac{\pi}{2}) \approx 0.050$ ,  $b(\arg(\beta) = \frac{\pi}{2}) \approx 78.65$ ,  $a(\arg(\beta) = \frac{\pi}{4}) \approx -0.057$ , and  $b(\arg(\beta) = \frac{\pi}{4}) \approx 198.11$ . The scaling is frozen below the lower critical length  $L_c \approx 14$ , limited by the bare asymmetric couplings  $t_a^\pm$  and  $t_b^\pm$ . Parameters are  $t_0 = 0.01$ ,  $t_1 = 0.75$ , and  $\delta_a = -\delta_b = 0.25$ , the same as those in Fig. 1.

To make progress in deriving the finite-size scaling properties of the  $\beta$ s, our strategy is to consider the large- $L$  limit and obtain the leading-order scaling behavior. In this limit, we can approximate the boundary equation (24) by retaining only the two dominant terms  $-X_{1,3}X_{2,4}(\beta_2\beta_4)^{L+1}$  and  $X_{1,2}X_{3,4}(\beta_3\beta_4)^{L+1}$ . To make

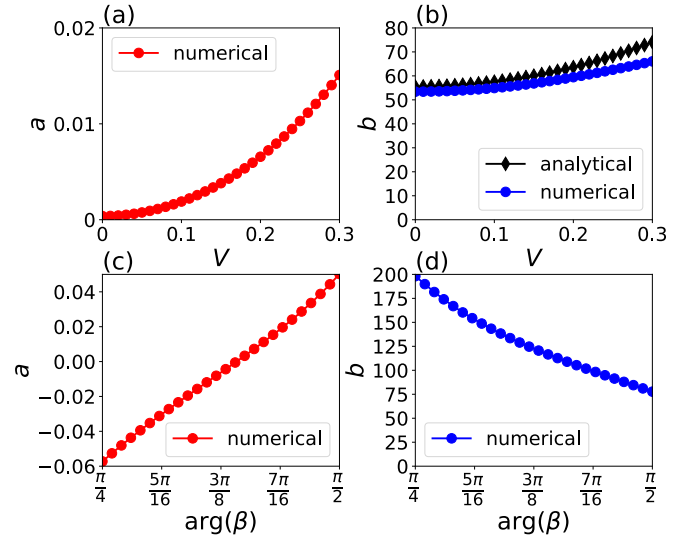


FIG. 5. (a), (b) Exponential scaling parameters  $a$  and  $b$  [Eq. (28)] of  $|\beta_3|$  as a function of  $V$  at  $\arg(\beta) = \frac{\pi}{2}$ . Their numerical values are extracted from the plot of  $|\beta_3|$  against  $L$ , which is computed from the numerical  $E_{\text{OBC}}$  data. In (b), this numerically obtained  $b$  is shown to be well predicted from the model parameters through the analytic result Eq. (29), which is derived under the small  $V$  approximation. (c), (d) Show the numerically obtained  $a$  and  $b$  as a function of  $\arg(\beta)$ , at fixed  $V = 0.5$ . Parameters are  $t_0 = 0.01$ ,  $t_1 = 0.75$ , and  $\delta_a = -\delta_b = 0.25$ , the same as those in Fig. 1.

further headway, we note that the cNHSE is already well manifested when the bare value of the coupling  $t_0$  is very small, i.e.,  $t_0 = 0.01$  as in Fig. 1. (In fact, if  $t_0$  is of the same order as the two Hatano-Nelson chains, it would be difficult to see the weak coupling/small- $L$  limit with real spectra.) As such, we can expand up to the second order of the coupling parameter  $t_0$  (see Appendix E) to obtain

$$\begin{aligned} \left| \frac{\beta_2}{\beta_3} \right| &\simeq \left| \frac{X_{1,2}X_{3,4}}{X_{1,3}X_{2,4}} \right|^{\frac{1}{L+1}} \\ &\approx \left| (t_a^+ t_b^- - t_a^- t_b^+) f_\infty(E_\infty) t_0^2 \right|^{\frac{1}{L+1}}, \end{aligned} \quad (26)$$

where  $E_\infty \equiv \lim_{L \rightarrow \infty} E_{\text{OBC}}$ , and

$$f_\infty(E_\infty) = \frac{\sqrt{(E_\infty - V)^2 - 4t_a^+ t_a^-} \sqrt{(E_\infty + V)^2 - 4t_b^+ t_b^-}}{h^2(E_\infty)}, \quad (27)$$

$h(E_\infty) = E_\infty^2(t_a^- - t_b^-)(t_a^+ - t_b^+) + (t_a^+ t_b^- - t_a^- t_b^+)^2 + 2E_\infty(t_a^+ t_a^- - t_b^+ t_b^-)V + (t_a^+ + t_b^+)(t_a^- + t_b^-)V^2$ . Notice that  $E_\infty$  in Eq. (26) depends on  $t_0$ . Equation (26) is Eq. (16) specialized to our coupled Hatano-Nelson model Hamiltonian [Eq. (18)]. It expresses the ratio of the GBZ quantities  $|\beta_2|$  and  $|\beta_3|$  as a constant exponentiated by  $1/(L+1)$ , which is a scaling behavior that is universal across cNHSE models.

While the  $1/(L+1)$  exponential scaling behavior holds generally for the ratio  $|\beta_M/\beta_{M+1}|$ , it can apply to  $|\beta_M|$

or  $|\beta_{M+1}|$  individually if they are related in special ways. In Fig. 4, we show the numerically extracted  $|\beta_2|$  and  $|\beta_3|$  at two special values of  $\arg(\beta)$ , where  $|\beta_2| \approx 1/|\beta_3|$  in Fig. 4(a) and  $|\beta_2|$  is constant in Fig. 4(b). As such,  $|\beta_2/\beta_3| \approx |\beta_2|^2 \approx |\beta_3|^{-2}$  in Fig. 4(a) and  $|\beta_2/\beta_3| \propto |\beta_3|^{-1}$  in Fig. 4(b), hence allowing for  $|\beta_3|$  to be fitted to an exponential form

$$|\beta_3| = a + b \frac{1}{L^{1+1}}, \quad (28)$$

where the parameters  $a, b \in \mathbb{R}$ ,  $b > 0$ , and  $|a| \ll 1 \ll |b|$ . In general, this exponential relation fits the numerically obtained  $|\beta|$ s very well for sufficiently large  $L$ , as demonstrated in Fig. 4. The actual values of fitting parameters  $a$  and  $b$  are shown in Fig. 5 as functions of the on-site energy  $V$  [Figs. 5(a) and 5(b)] and  $\arg(\beta)$  [Figs. 5(c) and 5(d)]. It is found that both  $a$  and  $b$  are monotonically increasing functions of the on-site energy  $V$  at  $\arg(\beta) = \frac{\pi}{2}$  [Figs. 5(a) and 5(b)]. Also, in the range of  $\arg(\beta) \in [\frac{\pi}{4}, \frac{\pi}{2}]$  for  $V = 0.5$ ,  $a$  is a monotonically increasing function of  $\arg(\beta)$ , but  $b$  is a monotonically decreasing function of  $\arg(\beta)$ . We see that the condition  $|a| \ll |b|$  is always satisfied with different on-site energy  $V$  and  $\arg(\beta)$ .

The correctness of our exponential fit can be checked by comparing against analytic results involving the model parameters. From Eq. (26), we see that in the case of  $|\beta_2| \approx 1/|\beta_3|$ , the parameter  $b$  in the exponential scaling relation is approximately given by

$$b \approx |(t_a^+ t_b^- - t_a^- t_b^+) f_\infty(E_\infty) t_0^2|^{-1/2}. \quad (29)$$

As shown in Fig. 5(b), both the analytical and numerical results agree well with each other when the on-site energy  $V$  is smaller than 0.2, where the  $|\beta_2| \approx 1/|\beta_3|$  approximation accurately holds. For different fixed  $\arg(\beta)$ ,  $E_{\text{OBC}}$  would be different, leading to different values of  $b$ . Indeed, as evident in Fig. 3(b), the convergence behavior of  $|\beta|$  and hence  $b$  varies significantly with  $\arg(\beta)$  [Fig. 5(d)].

## B. Lower critical system size for the cNHSE

As seen in Fig. 4, the scaling of the GBZ parameters  $|\beta_M|$  and  $|\beta_{M+1}|$  ( $M = 2$  here) is only exponential and described by Eq. (28) above a certain lower critical system size  $L_c$ . Below that, they remain effectively constant, indicative of the absence of the cNHSE. The reason is that the spatial skin decay lengths  $-1/\ln|\beta_M|$  and  $-1/\ln|\beta_{M+1}|$  cannot be faster than that of the physical NHSE chains in the cNHSE model. In our model, noting that  $|\beta_3| > |\beta_2|$ , we must have  $|\beta_{3c}| = \sqrt{t_a^+/t_a^-}$  and  $|\beta_{2c}| = \sqrt{t_b^+/t_b^-}$ , corresponding to the  $|\beta|$ s of the individual Hatano-Nelson chains.

Substituting  $|\beta_2/\beta_3|$  with  $|\beta_{2c}/\beta_{3c}|$  in Eq. (26), we obtain the critical system size  $L_c$  of our coupled Hatano-

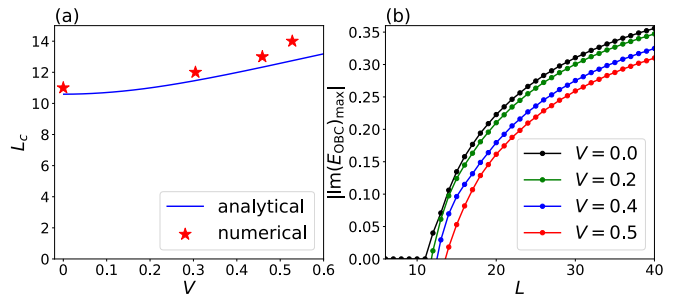


FIG. 6. (a) Critical system size  $L_c$  versus  $V$  at  $\arg(E_{\text{OBC}}) = \frac{\pi}{2}$ . The analytical result given by Eq. (30) (blue) agrees reasonably well with numerical results (red stars) estimated by the threshold system size  $L = L_c$ , below which the spectrum is unaffected by  $L$ . We observe that  $L_c$  increases with  $V$ , confirming the intuition that the inter-chain energy offset  $V$  obstructs critical NHSE hybridization. (b) Absolute value of the maximal imaginary part of the eigenvalues  $|\text{Im}(E_{\text{OBC}})_{\text{max}}|$  as a function of the system size  $L$ , also at  $\arg(E_{\text{OBC}}) = \frac{\pi}{2}$ . The onset of complex  $E_{\text{OBC}}$  typically occurs at  $L_c$ , except for small systems ( $L = 10$ ), where the nonzero  $V$  offset can give rise to complex energies [see Fig. 2(b)]. Parameters are  $t_0 = 0.01$ ,  $t_1 = 0.75$ , and  $\delta_a = -\delta_b = 0.25$ , the same as those in Fig. 1.

Nelson model as

$$L_c \approx \frac{2 \ln |(t_a^+ t_b^- - t_a^- t_b^+) f_\infty(E_\infty) t_0^2|}{\ln |t_b^+ t_a^- / (t_b^- t_a^+)|} - 1. \quad (30)$$

As shown in Fig. 6(a) for  $\arg(E_{\text{OBC}}) = \frac{\pi}{2}$ , this analytic expression [Eq. (30)] for  $L_c$  (blue curve) agrees rather well with its numerical determination (red stars), i.e., from plots such as Fig. 4. Not surprisingly, it increases monotonically with the inter-chain energy offset  $V$ , since the offset impedes energy matching and acts as an obstruction to the critical coupling between the Hatano-Nelson chains.

$L_c$  can also be thought of as the lower critical length above which the inter-chain coupling  $t_0$  is “switched on” to cause the cNHSE. As seen in Fig. 6(b), the energy spectrum becomes complex precisely above  $L_c$ . Since our OBC Hatano-Nelson chains have real spectra when uncoupled, it means that they become effectively coupled only when  $L \geq L_c$ . Naively, we would expect small  $t_0$  to continuously give rise to small imaginary energies; yet, in reality, there exists a sharp real-to-complex spectral transition [113, 127] controlled by  $L_c$ . We note that  $L_c \rightarrow \infty$  as  $t_0 \rightarrow 0$ , consistent with the expectation that uncoupled chains will never experience the cNHSE.

## IV. TOPOLOGICALLY COUPLED CHAIN MODEL

To complement the exposition of our coupled Hatano-Nelson cNHSE model above, we next consider more sophisticated inter-chain couplings which lead to size-controlled topological states, as first designed in [113].



In the basis  $C_{\mathbf{k}} = (c_{\mathbf{k},A}, c_{\mathbf{k},B})^T$ , it is given by

$$\mathcal{H}_{\text{top}}(z) = \begin{pmatrix} t_a^+ z + t_a^-/z + V & \delta_{ab}(z + 1/z) \\ -\delta_{ab}(z + 1/z) & t_b^+ z + t_b^-/z - V \end{pmatrix}, \quad (31)$$

where  $t_a^\pm = t_1 \pm \delta_a$ ,  $t_b^\pm = t_1 \pm \delta_b$ , and  $z = e^{ik}$ . Here, the simple inter-chain couplings  $t_0$  of the coupled Hatano-Nelson model are replaced by criss-crossing inter-chain couplings  $\pm\delta_{ab}$  which can potentially introduce topological flux [142]. Under PBCs, the energy eigenvalues can

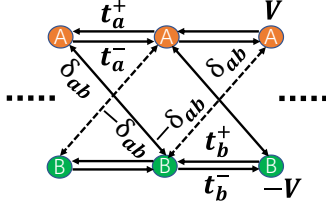


FIG. 7. Topologically coupled two-chain model [Eq. (33)] with criss-crossing inter-chain non-reciprocal couplings  $\pm\delta_{ab}$  and asymmetric hoppings  $t_a^\pm = t_1 \pm \delta_a$  and  $t_b^\pm = t_1 \pm \delta_b$  in chains A and B. The chains are given energy offsets of  $\pm V$ .

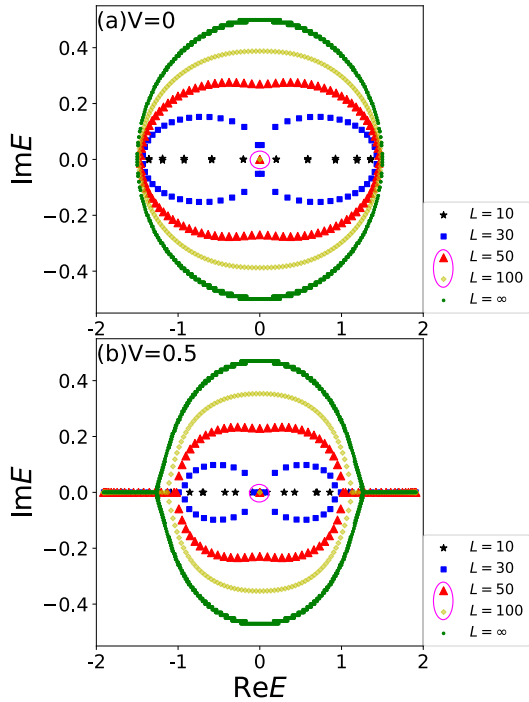


FIG. 8. OBC energy spectra of the topologically coupled chain model Hamiltonian (33) with (a)  $V = 0$  and (b)  $V = 0.5$  at different system sizes  $L = 10$  (black), 30 (blue), 50 (red), 100 (yellow),  $\infty$  (green). Notably, topological zero modes (circled) appear at  $E = 0$  in the point gap only at sufficiently large system sizes of  $L = 50, 100$ . The other parameters are  $\delta_{ab} = 0.5 \times 10^{-3}$ ,  $t_1 = 0.75$ , and  $\delta_a = -\delta_b = 0.25$ .

be simply obtained from the Hamiltonian (31) as

$$E_{\text{PBC}}^{(\pm)}(k) = 2t_1 \cos k + i(\delta_a + \delta_b) \sin k \pm \sqrt{[i(\delta_a - \delta_b) \sin k + V]^2 - 4\delta_{ab}^2 \cos^2 k}. \quad (32)$$

with  $k = -i \ln z \in \mathbb{R}$  and  $t_a^\pm = t_1 \pm \delta_a$ ,  $t_b^\pm = t_1 \pm \delta_b$ . By Fourier transformation, one obtains the real-space tight-binding Hamiltonian (Fig. 7):

$$H_t = \sum_n \left( t_a^+ c_{n,A}^\dagger c_{n+1,A} + t_a^- c_{n+1,A}^\dagger c_{n,A} + \delta_{ab} c_{n,A}^\dagger c_{n+1,B} - \delta_{ab} c_{n+1,B}^\dagger c_{n,A} + t_b^+ c_{n,B}^\dagger c_{n+1,B} + t_b^- c_{n+1,B}^\dagger c_{n,B} + \delta_{ab} c_{n+1,A}^\dagger c_{n,B} - \delta_{ab} c_{n,B}^\dagger c_{n+1,A} + V c_{n,A}^\dagger c_{n,A} - V c_{n,B}^\dagger c_{n,B} \right), \quad (33)$$

where  $c_{n,\alpha}$  ( $c_{n,\alpha}^\dagger$ ) is the annihilation (creation) operator on site  $\alpha$  ( $\alpha = A, B$ ) in cell  $n$ .

Following the similar derivations as Eq. (23), we can obtain the characteristic energy dispersion equation

$$(t_a^+ t_b^+ + \delta_{ab}^2) \beta^2 + [-(t_a^+ + t_b^+) E_{\text{OBC}} - (t_a^+ - t_b^+) V] \beta + (t_a^+ t_b^- + t_a^- t_b^+ + 2\delta_{ab}^2 + E_{\text{OBC}}^2 - V^2) + [-(t_a^- + t_b^-) E_{\text{OBC}} - (t_a^- - t_b^-) V] \beta^{-1} + (t_a^- t_b^- + \delta_{ab}^2) \beta^{-2} = 0. \quad (34)$$

Similarly as before, we can compute the OBC energy spectra and the GBZ of the topological coupled chain model Hamiltonian (33) at different finite system sizes  $L = 10, 30, 50, 100, \infty$  as shown in Figs. 8 and 9, respectively. We find that they are qualitatively similar to those of the coupled Hatano-Nelson model, except that there is a topological zero mode at  $E = 0$  (dirty red and yellow). These topological modes also correspond to isolated solutions in the GBZ plot (Fig. 9), although they are exempted from the finite-size scaling behavior. It is found that the topological zero modes appear at  $E = 0$  in the point gap only at sufficiently large system sizes as shown in Fig. 8. The reason is that the GBZ depends strongly on the system size as shown in Fig. 9, and so does the OBC spectrum as shown in Fig. 8. When we tune the system size  $L$  (regarding  $L$  as a parameter), the OBC spectrum changes. At a critical  $L$ , the OBC spectrum's gap closes and after that, topological zero modes appear, as shown in Fig. 13 in Appendix F. Different from the famous single-chain Su-Schrieffer-Heeger model [143–148], our topologically coupled chain model has two coupled chains, i.e., the coupling between these two chains plays an important role here. In the topologically coupled chain model, the competition between the coupling of the two chains and the finite system size determines the existence or absence of the topological zero modes. This conclusion can be found by calculating the topological phase diagram of the topologically coupled chain model as shown in Fig. 4(d) in a previous work [113]. Therefore, the strength of the coupling of the two chains

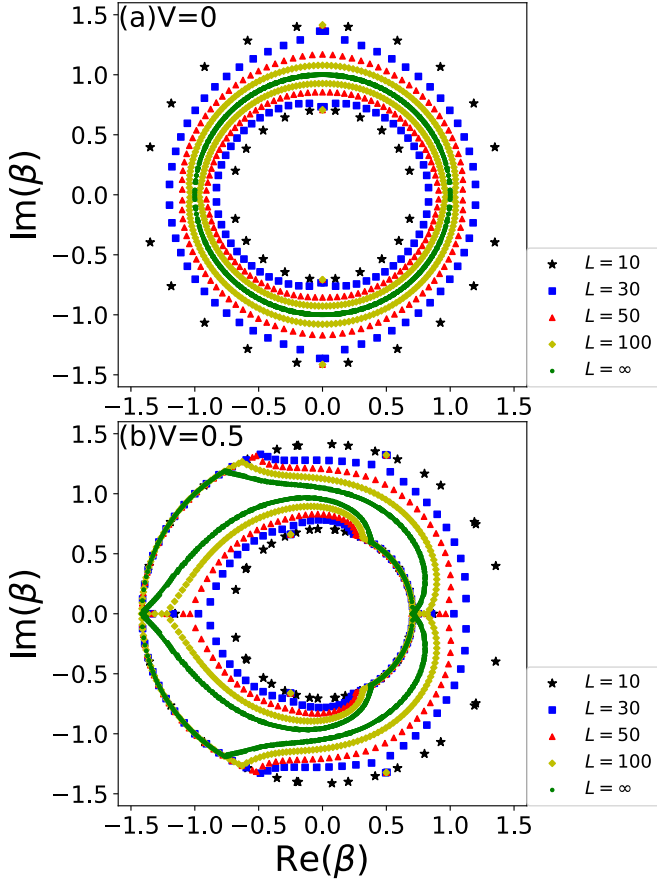


FIG. 9. GBZ of the topologically coupled chain model Hamiltonian (33) at different finite system sizes  $L = 10$  (black), 20 (blue), 50 (red), 100 (yellow),  $\infty$  (green) with (a)  $V = 0$  and (b)  $V = 0.5$ . Parameters are  $\delta_{ab} = 0.5 \times 10^{-3}$ ,  $t_1 = 0.75$ , and  $\delta_a = -\delta_b = 0.25$ , the same as those in Fig. 8. The GBZ is qualitatively similar to that in Fig. 3, apart from the isolated topological modes (dirty red and yellow) which by definition do not belong to any continuum of states.

determines the threshold system size which is required for the topological modes.

By enforcing OBCs in the real-space Hamiltonian, we arrive at

$$\begin{aligned} & \left[ Z_{1,4}^{(b)} Z_{2,3}^{(a)} (\beta_1 \beta_4)^{L+1} + Z_{1,4}^{(a)} Z_{2,3}^{(b)} (\beta_2 \beta_3)^{L+1} \right] \\ & - \left[ Z_{1,3}^{(b)} Z_{2,4}^{(a)} (\beta_1 \beta_3)^{L+1} + Z_{1,3}^{(a)} Z_{2,4}^{(b)} (\beta_2 \beta_4)^{L+1} \right] \\ & + \left[ Z_{1,2}^{(b)} Z_{3,4}^{(a)} (\beta_1 \beta_2)^{L+1} + Z_{1,2}^{(a)} Z_{3,4}^{(b)} (\beta_3 \beta_4)^{L+1} \right] = 0, \end{aligned} \quad (35)$$

where dispersion relation solutions  $\beta_j$  ( $j = 1, 2, 3, 4$ ) are arranged so that  $|\beta_1| \leq |\beta_2| \leq |\beta_3| \leq |\beta_4|$ , and  $Z_{i,j}^{(c)}$  ( $i, j = 1, 2, 3, 4$ ;  $c = a, b$ ) are defined as

$$Z_{i,j}^{(c)} = X_i^{(c)} Y_j^{(c)} - X_j^{(c)} Y_i^{(c)}. \quad (36)$$

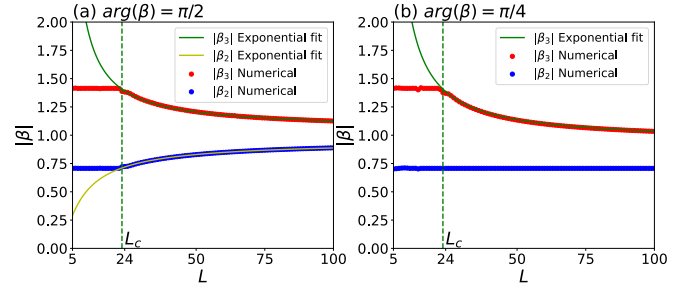


FIG. 10. The GBZ radii  $|\beta_2|$  and  $|\beta_3|$  of the topologically coupled chain model Hamiltonian (33) versus the system size  $L$  at (a)  $\arg(\beta) = \frac{\pi}{2}$  and (b)  $\arg(\beta) = \frac{\pi}{4}$ . The exponential fits of  $|\beta_3|$  correspond to scaling parameters  $a(\arg(\beta) = \frac{\pi}{2}) \approx 0.0520$ ,  $b(\arg(\beta) = \frac{\pi}{2}) \approx 1476.563$ ,  $a(\arg(\beta) = \frac{\pi}{4}) \approx -0.0607$ , and  $b(\arg(\beta) = \frac{\pi}{4}) \approx 8791.616$ . The cNHSE scaling is frozen below  $L = L_c \approx 23$ , but at  $\arg(\beta) = \frac{\pi}{4}$ ,  $|\beta_2|$  remains constant across all  $L$ . Here,  $V = 0.5$  and the other parameters  $\delta_{ab} = 0.5 \times 10^{-3}$ ,  $t_1 = 0.75$ , and  $\delta_a = -\delta_b = 0.25$  are the same as those in Fig. 9.

Here,  $X_j^{(c)}$  and  $Y_j^{(c)}$  are defined as

$$X_j^{(a)} = E_{\text{OBC}} - (t_a^+ - t_a^-) \beta_j - V, \quad (37)$$

$$Y_j^{(a)} = E_{\text{OBC}} - (t_b^+ - t_b^-) \beta_j + V, \quad (38)$$

$$X_j^{(b)} = E_{\text{OBC}} + (t_a^+ - t_a^-) \beta_j^{-1} - V, \quad (39)$$

$$Y_j^{(b)} = E_{\text{OBC}} + (t_b^+ - t_b^-) \beta_j^{-1} + V. \quad (40)$$

The corresponding derivation of Eq. (35) is given in Appendix G.

To deal with Eq. (35), we only consider the two dominant terms  $-Z_{1,3}^{(a)} Z_{2,4}^{(b)} (\beta_2 \beta_4)^{L+1}$  and  $Z_{1,2}^{(a)} Z_{3,4}^{(b)} (\beta_3 \beta_4)^{L+1}$  on the left-hand side. In this case, by substituting the solutions of the characteristic equation (34) into this approximated boundary equation, we can approximate Eq. (35) as

$$\begin{aligned} \left| \frac{\beta_2}{\beta_3} \right| & \simeq \left| \frac{Z_{1,2}^{(a)} Z_{3,4}^{(b)}}{Z_{1,3}^{(a)} Z_{2,4}^{(b)}} \right|_{E_{\text{OBC}}=E_\infty}^{\frac{1}{L+1}} \\ & \approx \left| \frac{\Delta_a (E_\infty - V + \Delta_a) \Delta_b (E_\infty + V + \Delta_b)}{2t_a^+ t_b^- [V^2 - E_\infty^2 + 2(t_a^+ t_b^- + t_b^+ t_a^-) + \Delta_a \Delta_b]} \right|^{\frac{1}{L+1}}, \end{aligned} \quad (41)$$

where  $\Delta_a = \sqrt{(E_\infty - V)^2 - 4t_a^+ t_a^-}$ ,  $\Delta_b = \sqrt{(E_\infty + V)^2 - 4t_b^+ t_b^-}$ , and we have used the approximation  $\delta_{ab} \rightarrow 0$  under the condition of weak inter-chain couplings. Notice that  $E_\infty$  in Eq. (41) depends on  $\delta_{ab}$ . Therefore, we can also follow Eq. (28) and postulate an exponential fitting ansatz of  $|\beta_3|$  as

$$|\beta_3| = a + b \frac{1}{L+1}, \quad (42)$$

for cases where  $|\beta_2| \approx 1/|\beta_3|$ . The scaling behavior of  $a$  and  $b$  in Eq. (42) can be extracted or estimated from the asymptotic result Eq. (41) with the model parameters.

In Figs. 10(a) and 10(b), we show  $|\beta_2|$  and  $|\beta_3|$  for the topologically coupled chain model Hamiltonian (33) as a function of the system size  $L$  both from the exponential formula in Eq. (42) and from numerical diagonalization. We observe an exponential scaling behavior qualitatively similar to that of the coupled Hatano-Nelson model, which should also universally holds for other cNHSE models.

## V. ROBUST SPECTRAL SCALING BEHAVIOR UNDER DISORDER

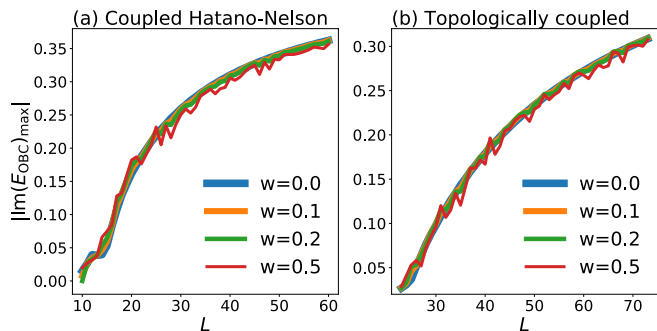


FIG. 11. Absolute value of the maximal imaginary part of the eigenvalues  $|\text{Im}(E_{\text{OBC}})_{\text{max}}|$  for different system sizes  $L$ , which is satisfied for the eigenenergy with  $\arg(E_{\text{OBC}}) = \frac{\pi}{2}$ . In both (a) the coupled Hatano-Nelson model [Eq. (18)] and (b) the topologically coupled chain model [Eq. (33)], the spectral scaling behavior is very robust up to disorder strength  $w = 0.2$ , as defined in Eq. (43). Even at much larger disorder  $w = 0.5$ , the same qualitative spectral scaling prevails. Here,  $V = 0.5$  and the other parameters are  $t_0 = 0.01$ ,  $\delta_{ab} = 0.5 \times 10^{-3}$ ,  $t_1 = 0.75$ , and  $\delta_a = -\delta_b = 0.25$ , the same as those in previous figures on these respective models.

In this section, we check the robustness of the scaling behavior of the OBC spectra in the presence of uniformly distributed on-site disorder

$$H_{\text{dis}} = \sum_{n,\alpha} \tilde{w}(n, \alpha) c_{n,\alpha}^\dagger c_{n,\alpha} \quad (43)$$

with random number  $\tilde{w} \in [-w/2, w/2]$  and  $\alpha = A, B$  are the site indices in the cell  $n$ . Since the GBZ is directly determined through the OBC spectrum, robustness in the scaling behavior in the spectrum would also imply similar robustness in the GBZ.

In Fig. 11, we plot the absolute value of the maximal imaginary part of the eigenenergies  $|\text{Im}(E_{\text{OBC}})_{\text{max}}|$  as a function of the system size  $L$  under different disorder strengths from  $w = 0$  to  $0.5$ .  $|\text{Im}(E_{\text{OBC}})_{\text{max}}|$  determines the “width” of the spectrum in the imaginary direction and can be used as a measure of how the shape of the spectrum is deformed under disorder. For our models,  $|\text{Im}(E_{\text{OBC}})_{\text{max}}|$  usually occurs when  $\arg(E_{\text{OBC}}) = \frac{\pi}{2}$ , but that is not necessarily universal. From Fig. 11, we find

that relatively weak disorder ( $w < 0.2$ ) affects the spectrum negligibly, but moderately large disorder ( $w = 0.5$ ) gives rise to visible spectral perturbations. However, the qualitative spectral scaling behavior remains very robust, which indicates that the cNHSE is strongly robust against on-site disorder. This is not surprising given that the cNHSE arises from the competition between different NHSE channels, and should not be affected too much by the on-site energy landscape. It has to be noted that *hopping* disorder, however, can affect the long-time state dynamics and hence significantly modify the overall energy spectrum [126, 149–152].

## VI. DISCUSSION

Systems experiencing the critical non-Hermitian skin effect (cNHSE) are particularly sensitive to the system size, exhibiting qualitatively different spectra and spatial eigenstate behavior at different sizes  $L$ . How the cNHSE scaling is exactly described by the GBZ, particularly for a system of finite size, is an open question. As we already know, the GBZ can be used to restore the BBC in the thermodynamic limit. But for a system of finite size, can GBZ still be a valid theoretical framework? Using the GBZ as a tool to investigate the cNHSE scaling behavior provides an effective way to understand the physical picture of the finite-size effect on the competing NHSE tendencies between small and large size limits.

In this work, we considered a generic two-component cNHSE ansatz model with two competing NHSE channels, and provided detailed studies of two paradigmatic models, of which the minimal model studied by Ref. [127] is a special case. We find that our effective finite-size GBZ obeys a universal exponential scaling law, with exponent inversely proportional to the system size, and scaling rate  $b$  expressible in term of the model parameters in certain cases. Based on this, we provide detailed and empirically verified estimates of the critical system size  $L_c$  where such a scaling relation begins to hold both analytically and numerically.

Such cNHSE phenomena can be readily experimentally demonstrated in non-Hermitian metamaterials with well-controlled gain/loss and effective couplings, such as photonic crystal arrays and electrical circuits. Since the non-reciprocity from different NHSE can cancel, the setup may not even require physical asymmetric couplings, such as in the recent experiment [52]. Moving forward, it would be immensely interesting to explore the interplay of cNHSE and many-body interactions in emerging and rapidly progressing platforms such as ultracold atomic arrays and quantum circuits.

## ACKNOWLEDGMENTS

We thank Zhesen Yang, Kai Zhang, and Chen Fang for helpful discussions. F.Q. is supported by the Singapore

- 
- [1] Q. Zhong, J. Ren, M. Khajavikhan, D. N. Christodoulides, Ş. K. Özdemir, and R. El-Ganainy, “Sensing with exceptional surfaces in order to combine sensitivity with robustness,” *Phys. Rev. Lett.* **122**, 153902 (2019).
- [2] P. Djorwe, Yan Pennec, and Bahram Djafari-Rouhani, “Exceptional point enhances sensitivity of optomechanical mass sensors,” *Physical Review Applied* **12**, 024002 (2019).
- [3] Zhiwei Guo, Tengzhou Zhang, Juan Song, Haitao Jiang, and Hong Chen, “Sensitivity of topological edge states in a non-hermitian dimer chain,” *Photonics Research* **9**, 574–582 (2021).
- [4] Changdong Chen, Yijun Xie, and Shu-Wei Huang, “Nanophotonic optical gyroscope with sensitivity enhancement around mirrored exceptional points,” *Optics Communications* **483**, 126674 (2021).
- [5] Chong Chen, Liang Jin, and Ren-Bao Liu, “Sensitivity of parameter estimation near the exceptional point of a non-hermitian system,” *New Journal of Physics* **21**, 083002 (2019).
- [6] Alireza Nikzamir, Kasra Rouhi, Alexander Figotin, and Filippo Capolino, “How to achieve exceptional points in coupled resonators using a gyrator or  $pt$ -symmetry, and in a time-modulated single resonator: high sensitivity to perturbations,” *EPJ Applied Metamaterials* **9**, 14 (2022).
- [7] Ching Hua Lee, “Exceptional bound states and negative entanglement entropy,” *Physical Review Letters* **128**, 010402 (2022).
- [8] Po-Yao Chang, Jhih-Shih You, Xueda Wen, and Shin-sei Ryu, “Entanglement spectrum and entropy in topological non-hermitian systems and nonunitary conformal field theory,” *Physical Review Research* **2**, 033069 (2020).
- [9] Balázs Dóra, Doru Sticlet, and Cătălin Paşcu Moca, “Correlations at  $pt$ -symmetric quantum critical point,” *Physical Review Letters* **128**, 146804 (2022).
- [10] Yi-Cheng Wang, HH Jen, and Jhih-Shih You, “Scaling laws for non-hermitian skin effect with long-range couplings,” *arXiv preprint arXiv:2211.16565* (2022).
- [11] Hengyun Zhou, Jong Yeon Lee, Shang Liu, and Bo Zhen, “Exceptional surfaces in  $pt$ -symmetric non-hermitian photonic systems,” *Optica* **6**, 190–193 (2019).
- [12] Xiao Zhang, Guangjie Li, Yuhan Liu, Tommy Tai, Ronny Thomale, and Ching Hua Lee, “Tidal surface states as fingerprints of non-hermitian nodal knot metals,” *Communications Physics* **4**, 47 (2021).
- [13] Jan Wiersig, “Robustness of exceptional-point-based sensors against parametric noise: The role of hamiltonian and liouvillian degeneracies,” *Phys. Rev. A* **101**, 053846 (2020).
- [14] Jan Wiersig, “Prospects and fundamental limits in exceptional point-based sensing,” *Nature communications* **11**, 1–3 (2020).
- [15] Jan Wiersig, “Review of exceptional point-based sensors,” *Photonics Research* **8**, 1457–1467 (2020).
- [16] Gui-Lei Zhu, Amir Targholizadeh, Xin-You Lu, Cem Yuce, and Hamidreza Ramezani, “Exceptional point generated robust asymmetric high-order harmonics,” *arXiv preprint arXiv:2201.07663* (2022).
- [17] Lei Xiao, Tianshu Deng, Kunkun Wang, Zhong Wang, Wei Yi, and Peng Xue, “Observation of non-bloch parity-time symmetry and exceptional points,” *Physical Review Letters* **126**, 230402 (2021).
- [18] Yuto Ashida, Zongping Gong, and Masahito Ueda, “Non-hermitian physics,” *Advances in Physics* **69**, 249–435 (2020).
- [19] Ramy El-Ganainy, Konstantinos G Makris, Mercedeh Khajavikhan, Ziad H Musslimani, Stefan Rotter, and Demetrios N Christodoulides, “Non-hermitian physics and  $pt$  symmetry,” *Nature Physics* **14**, 11–19 (2018).
- [20] Kohei Kawabata, Ken Shiozaki, Masahito Ueda, and Masatoshi Sato, “Symmetry and topology in non-hermitian physics,” *Physical Review X* **9**, 041015 (2019).
- [21] Emil J Bergholtz, Jan Carl Budich, and Flore K Kunst, “Exceptional topology of non-hermitian systems,” *Reviews of Modern Physics* **93**, 015005 (2021).
- [22] Masaya Nakagawa and Norio Kawakami, “Nonequilibrium topological phase transitions in two-dimensional optical lattices,” *Physical Review A* **89**, 013627 (2014).
- [23] Lei Xiao, Tianshu Deng, Kunkun Wang, Gaoyan Zhu, Zhong Wang, Wei Yi, and Peng Xue, “Non-hermitian bulk–boundary correspondence in quantum dynamics,” *Nature Physics* **16**, 761–766 (2020).
- [24] Fei Song, Shunyu Yao, and Zhong Wang, “Non-hermitian skin effect and chiral damping in open quantum systems,” *Physical review letters* **123**, 170401 (2019).
- [25] Lin Zhang, Wei Jia, and Xiong-Jun Liu, “Universal topological quench dynamics: Altland-zirnbauer tenfold classes,” *arXiv preprint arXiv:2104.00617* (2021).
- [26] Danying Yu, Bo Peng, Xianfeng Chen, Xiong-Jun Liu, and Luqi Yuan, “Topological holographic quench dynamics in a synthetic frequency dimension,” *Light: Science & Applications* **10**, 209 (2021).
- [27] Wei Jia, Lin Zhang, Long Zhang, and Xiong-Jun Liu, “Dynamically characterizing topological phases by high-order topological charges,” *Physical Review A* **103**, 052213 (2021).
- [28] Lin Zhang, Long Zhang, and Xiong-Jun Liu, “Quench-induced dynamical topology under dynamical noise,” *Phys. Rev. Research* **3**, 013229 (2021).
- [29] Xiang-Long Yu, Wentao Ji, Lin Zhang, Ya Wang, Jian-sheng Wu, and Xiong-Jun Liu, “Quantum dynamical characterization and simulation of topological phases with high-order band inversion surfaces,” *PRX Quantum* **2**, 020320 (2021).
- [30] Long Zhang, Lin Zhang, and Xiong-Jun Liu, “Unified theory to characterize floquet topological phases by quench dynamics,” *Physical Review Letters* **125**, 183001 (2020).
- [31] Chang-Rui Yi, Long Zhang, Lin Zhang, Rui-Heng Jiao, Xiang-Can Cheng, Zong-Yao Wang, Xiao-Tian Xu, Wei Sun, Xiong-Jun Liu, Shuai Chen, *et al.*, “Observing topological charges and dynamical bulk-surface corre-



- spondence with ultracold atoms,” *Physical review letters* **123**, 190603 (2019).
- [32] Ya Wang, Wentao Ji, Zihua Chai, Yuhang Guo, Mengqi Wang, Xiangyu Ye, Pei Yu, Long Zhang, Xi Qin, Pengfei Wang, *et al.*, “Experimental observation of dynamical bulk-surface correspondence in momentum space for topological phases,” *Physical Review A* **100**, 052328 (2019).
  - [33] Long Zhang, Lin Zhang, Ying Hu, Sen Niu, and Xiong-Jun Liu, “Nonequilibrium characterization of equilibrium correlated quantum phases,” *Physical Review B* **103**, 224308 (2021).
  - [34] Wei Sun, Chang-Rui Yi, Bao-Zong Wang, Wei-Wei Zhang, Barry C Sanders, Xiao-Tian Xu, Zong-Yao Wang, Joerg Schmiedmayer, Youjin Deng, Xiong-Jun Liu, *et al.*, “Uncover topology by quantum quench dynamics,” *Physical review letters* **121**, 250403 (2018).
  - [35] Lin Zhang, Long Zhang, Sen Niu, and Xiong-Jun Liu, “Dynamical classification of topological quantum phases,” *Science Bulletin* **63**, 1385–1391 (2018).
  - [36] Jiaming Li, Andrew K Harter, Ji Liu, Leonardo de Melo, Yogesh N Joglekar, and Le Luo, “Observation of parity-time symmetry breaking transitions in a dissipative floquet system of ultracold atoms,” *Nature communications* **10**, 1–7 (2019).
  - [37] Samantha Lapp, Jackson Ang’ong’a, Fangzhao Alex An, and Bryce Gadway, “Engineering tunable local loss in a synthetic lattice of momentum states,” *New Journal of Physics* **21**, 045006 (2019).
  - [38] Zejian Ren, Dong Liu, Entong Zhao, Chengdong He, Ka Kwan Pak, Jensen Li, and Gyu-Boong Jo, “Chiral control of quantum states in non-hermitian spin-orbit-coupled fermions,” *Nature Physics* **18**, 385–389 (2022).
  - [39] Qian Liang, Dizhou Xie, Zhaoli Dong, Haowei Li, Hang Li, Bryce Gadway, Wei Yi, and Bo Yan, “Dynamic signatures of non-hermitian skin effect and topology in ultracold atoms,” *Phys. Rev. Lett.* **129**, 070401 (2022).
  - [40] Wei Gou, Tao Chen, Dizhou Xie, Teng Xiao, Tian-Shu Deng, Bryce Gadway, Wei Yi, and Bo Yan, “Tunable nonreciprocal quantum transport through a dissipative aharonov-bohm ring in ultracold atoms,” *Physical review letters* **124**, 070402 (2020).
  - [41] Tobias Helbig, Tobias Hofmann, S Imhof, M Abdelghany, T Kiessling, LW Molenkamp, CH Lee, A Szaameit, M Greiter, and R Thomale, “Generalized bulk-boundary correspondence in non-hermitian topoelectrical circuits,” *Nature Physics* **16**, 747–750 (2020).
  - [42] Tobias Hofmann, Tobias Helbig, Ching Hua Lee, Martin Greiter, and Ronny Thomale, “Chiral voltage propagation and calibration in a topoelectrical chern circuit,” *Physical review letters* **122**, 247702 (2019).
  - [43] Shuo Liu, Shaojie Ma, Cheng Yang, Lei Zhang, Wenlong Gao, Yuan Jiang Xiang, Tie Jun Cui, and Shuang Zhang, “Gain-and loss-induced topological insulating phase in a non-hermitian electrical circuit,” *Physical Review Applied* **13**, 014047 (2020).
  - [44] Shuo Liu, Ruiwen Shao, Shaojie Ma, Lei Zhang, Oubo You, Haotian Wu, Yuan Jiang Xiang, Tie Jun Cui, and Shuang Zhang, “Non-hermitian skin effect in a non-hermitian electrical circuit,” *Research* **2021**, 5608038 (2021).
  - [45] Deyuan Zou, Tian Chen, Wenjing He, Jiacheng Bao, Ching Hua Lee, Houjun Sun, and Xiangdong Zhang, “Observation of hybrid higher-order skin-topological effect in non-hermitian topoelectrical circuits,” *Nature Communications* **12**, 7201 (2021).
  - [46] Alexander Stegmaier, Stefan Imhof, Tobias Helbig, Tobias Hofmann, Ching Hua Lee, Mark Kremer, Alexander Fritzsche, Thorsten Feichtner, Sebastian Klemmt, Sven Höfling, *et al.*, “Topological defect engineering and p t symmetry in non-hermitian electrical circuits,” *Physical Review Letters* **126**, 215302 (2021).
  - [47] Hendrik Hohmann, Tobias Hofmann, Tobias Helbig, Stefan Imhof, Hauke Brand, Lavi K Upreti, Alexander Stegmaier, Alexander Fritzsche, Tobias Müller, Udo Schwingenschlögl, *et al.*, “Observation of cnoidal wave localization in non-linear topoelectric circuits,” *arXiv preprint arXiv:2206.09931* (2022).
  - [48] Bo Lv, Rui Chen, Rujiang Li, Chunying Guan, Bin Zhou, Guohua Dong, Chao Zhao, YiCheng Li, Ying Wang, Huibin Tao, *et al.*, “Realization of quasicrystalline quadrupole topological insulators in electrical circuits,” *Communications Physics* **4**, 108 (2021).
  - [49] Xiao Zhang, Boxue Zhang, Haydar Sahin, Zhuo Bin Siu, SM Rafi-Ul-Islam, Jian Feng Kong, Mansoor Jalil, Ronny Thomale, and Ching Hua Lee, “Anomalous fractal scaling in two-dimensional electric networks,” *arXiv preprint arXiv:2204.05329* (2022).
  - [50] Patrick M Lenggenhager, Alexander Stegmaier, Lavi K Upreti, Tobias Hofmann, Tobias Helbig, Achim Vollhardt, Martin Greiter, Ching Hua Lee, Stefan Imhof, Hauke Brand, *et al.*, “Simulating hyperbolic space on a circuit board,” *Nature Communications* **13**, 1–8 (2022).
  - [51] Ce Shang, Shuo Liu, Ruiwen Shao, Peng Han, Xiaoning Zang, Xiangliang Zhang, Khaled Nabil Salama, Wenlong Gao, Ching Hua Lee, Ronny Thomale, *et al.*, “Experimental identification of the second-order non-hermitian skin effect with physics-graph-informed machine learning,” *Advanced Science* **9**, 2202922 (2022).
  - [52] Xiao Zhang, Boxue Zhang, Weihong Zhao, and Ching Hua Lee, “Observation of non-local impedance response in a passive electrical circuit,” *arXiv preprint arXiv:2211.09152* (2022).
  - [53] Maopeng Wu, Qian Zhao, Lei Kang, Mingze Weng, Zhonghai Chi, Ruiguang Peng, Jingquan Liu, Douglas H. Werner, Yonggang Meng, and Ji Zhou, “Evidencing non-bloch dynamics in temporal topoelectrical circuits,” *Phys. Rev. B* **107**, 064307 (2023).
  - [54] Federico Roccati, Salvatore Lorenzo, Giuseppe Calajò, G Massimo Palma, Angelo Carollo, and Francesco Ciccarello, “Exotic interactions mediated by a non-hermitian photonic bath,” *Optica* **9**, 565–571 (2022).
  - [55] Liang Feng, Ramy El-Ganainy, and Li Ge, “Non-hermitian photonics based on parity-time symmetry,” *Nature Photonics* **11**, 752–762 (2017).
  - [56] Lawrence D Tzuang, Kejie Fang, Paulo Nussenzveig, Shanhui Fan, and Michal Lipson, “Non-reciprocal phase shift induced by an effective magnetic flux for light,” *Nature photonics* **8**, 701–705 (2014).
  - [57] Hengyun Zhou, Chao Peng, Yoseob Yoon, Chia Wei Hsu, Keith A Nelson, Liang Fu, John D Joannopoulos, Marin Soljačić, and Bo Zhen, “Observation of bulk fermi arc and polarization half charge from paired exceptional points,” *Science* **359**, 1009–1012 (2018).
  - [58] Bo Zhen, Chia Wei Hsu, Yuichi Igarashi, Ling Lu, Ido Kaminer, Adi Pick, Song-Liang Chua, John D Joannopoulos, and Marin Soljačić, “Spawning rings of exceptional points out of dirac cones,” *Nature* **525**, 354–

- 358 (2015).
- [59] Julia M Zeuner, Mikael C Rechtsman, Yonatan Plotnik, Yaakov Lumer, Stefan Nolte, Mark S Rudner, Mordechai Segev, and Alexander Szameit, “Observation of a topological transition in the bulk of a non-hermitian system,” *Physical review letters* **115**, 040402 (2015).
  - [60] Mohammad-Ali Miri and Andrea Alù, “Exceptional points in optics and photonics,” *Science* **363**, eaar7709 (2019).
  - [61] Liang Feng, Maurice Ayache, Jingqing Huang, Ye-Long Xu, Ming-Hui Lu, Yan-Feng Chen, Yeshaiah Fainman, and Axel Scherer, “Nonreciprocal light propagation in a silicon photonic circuit,” *Science* **333**, 729–733 (2011).
  - [62] Zhen Shen, Yan-Lei Zhang, Yuan Chen, Chang-Ling Zou, Yun-Feng Xiao, Xu-Bo Zou, Fang-Wen Sun, Guang-Can Guo, and Chun-Hua Dong, “Experimental realization of optomechanically induced non-reciprocity,” *Nature Photonics* **10**, 657–661 (2016).
  - [63] Kun Ding, Guancong Ma, Meng Xiao, ZQ Zhang, and Che Ting Chan, “Emergence, coalescence, and topological properties of multiple exceptional points and their experimental realization,” *Physical Review X* **6**, 021007 (2016).
  - [64] Weiyuan Tang, Xue Jiang, Kun Ding, Yi-Xin Xiao, Zhao-Qing Zhang, Che Ting Chan, and Guancong Ma, “Exceptional nexus with a hybrid topological invariant,” *Science* **370**, 1077–1080 (2020).
  - [65] Kun Ding, Guancong Ma, ZQ Zhang, and Che Ting Chan, “Experimental demonstration of an anisotropic exceptional point,” *Physical review letters* **121**, 085702 (2018).
  - [66] Weiyuan Tang, Kun Ding, and Guancong Ma, “Direct measurement of topological properties of an exceptional parabola,” *Physical Review Letters* **127**, 034301 (2021).
  - [67] Weiyuan Tang, Kun Ding, and Guancong Ma, “Experimental realization of non-abelian permutations in a three-state non-hermitian system,” *National Science Review* **9**, nwac010 (2022).
  - [68] Sang Hyun Park, Sung-Gyu Lee, Soojeong Baek, Tae-woo Ha, Sanghyub Lee, Bumki Min, Shuang Zhang, Mark Lawrence, and Teun-Teun Kim, “Observation of an exceptional point in a non-hermitian metasurface,” *Nanophotonics* **9**, 1031–1039 (2020).
  - [69] Corentin Coullais, Dimitrios Sounas, and Andrea Alu, “Static non-reciprocity in mechanical metamaterials,” *Nature* **542**, 461–464 (2017).
  - [70] Weiwei Zhu, Xincheng Fang, Dongting Li, Yong Sun, Yong Li, Yun Jing, and Hong Chen, “Simultaneous observation of a topological edge state and exceptional point in an open and non-hermitian acoustic system,” *Physical review letters* **121**, 124501 (2018).
  - [71] Ananya Ghatak, Martin Brandenbourger, Jasper Van Wezel, and Corentin Coullais, “Observation of non-hermitian topology and its bulk–edge correspondence in an active mechanical metamaterial,” *Proceedings of the National Academy of Sciences* **117**, 29561–29568 (2020).
  - [72] Martin Brandenbourger, Xander Locsin, Edan Lerner, and Corentin Coullais, “Non-reciprocal robotic metamaterials,” *Nature communications* **10**, 1–8 (2019).
  - [73] He Gao, Haoran Xue, Zhongming Gu, Tuo Liu, Jie Zhu, and Baile Zhang, “Non-hermitian route to higher-order topology in an acoustic crystal,” *Nature communications* **12**, 1888 (2021).
  - [74] Fang Qin, Ching Hua Lee, Rui Chen, *et al.*, “Light-induced phase crossovers in a quantum spin hall system,” *Physical Review B* **106**, 235405 (2022).
  - [75] Jiawei Wang, Sreeramulu Valligatla, Yin Yin, Lukas Schwarz, Mariana Medina-Sánchez, Stefan Baunack, Ching Hua Lee, Ronny Thomale, Shilong Li, Vladimir M Fomin, *et al.*, “Experimental observation of berry phases in optical möbius-strip microcavities,” *Nature Photonics* **17**, 120–125 (2023).
  - [76] Zhongming Gu, He Gao, Pei-Chao Cao, Tuo Liu, Xue-Feng Zhu, and Jie Zhu, “Controlling sound in non-hermitian acoustic systems,” *Physical Review Applied* **16**, 057001 (2021).
  - [77] Fang Qin, Rui Chen, and Hai-Zhou Lu, “Phase transitions in intrinsic magnetic topological insulator with high-frequency pumping,” *Journal of Physics: Condensed Matter* **34**, 225001 (2022).
  - [78] Xinhua Wen, Xinghong Zhu, Alvin Fan, Wing Yim Tam, Jie Zhu, Hong Wei Wu, Fabrice Lemoult, Mathias Fink, and Jensen Li, “Unidirectional amplification with acoustic non-hermitian space- time varying metamaterial,” *Communications Physics* **5**, 1–7 (2022).
  - [79] Fang Qin, Shuai Li, ZZ Du, CM Wang, Wenqing Zhang, Dapeng Yu, Hai-Zhou Lu, XC Xie, *et al.*, “Theory for the charge-density-wave mechanism of 3d quantum hall effect,” *Physical Review Letters* **125**, 206601 (2020).
  - [80] Abhishek Gupta and Ramathasan Thevamaran, “Requisites on viscoelasticity for exceptional points in passive elastodynamic metamaterials,” *arXiv preprint arXiv:2209.04960* (2022).
  - [81] Ching-Kai Chiu, Hong Yao, and Shinsei Ryu, “Classification of topological insulators and superconductors in the presence of reflection symmetry,” *Phys. Rev. B* **88**, 075142 (2013).
  - [82] Ching-Kai Chiu, Jeffrey C. Y. Teo, Andreas P. Schnyder, and Shinsei Ryu, “Classification of topological quantum matter with symmetries,” *Rev. Mod. Phys.* **88**, 035005 (2016).
  - [83] Andrew C. Potter, Takahiro Morimoto, and Ashvin Vishwanath, “Classification of interacting topological floquet phases in one dimension,” *Phys. Rev. X* **6**, 041001 (2016).
  - [84] Maissam Barkeshli, Chao-Ming Jian, and Xiao-Liang Qi, “Classification of topological defects in abelian topological states,” *Phys. Rev. B* **88**, 241103 (2013).
  - [85] Max McGinley and Nigel R. Cooper, “Classification of topological insulators and superconductors out of equilibrium,” *Phys. Rev. B* **99**, 075148 (2019).
  - [86] Dominic V. Else and Chetan Nayak, “Classification of topological phases in periodically driven interacting systems,” *Phys. Rev. B* **93**, 201103 (2016).
  - [87] Shunyu Yao and Zhong Wang, “Edge states and topological invariants of non-hermitian systems,” *Physical review letters* **121**, 086803 (2018).
  - [88] Ye Xiong, “Why does bulk boundary correspondence fail in some non-hermitian topological models,” *Journal of Physics Communications* **2**, 035043 (2018).
  - [89] Ching Hua Lee and Ronny Thomale, “Anatomy of skin modes and topology in non-hermitian systems,” *Physical Review B* **99**, 201103 (2019).
  - [90] Flore K Kunst, Elisabet Edvardsson, Jan Carl Budich, and Emil J Bergholtz, “Biorthogonal bulk-boundary correspondence in non-hermitian systems,” *Physical review letters* **121**, 026808 (2018).

- [91] Kazuki Yokomizo and Shuichi Murakami, “Non-bloch band theory of non-hermitian systems,” *Phys. Rev. Lett.* **123**, 066404 (2019).
- [92] Ken-Ichiro Imura and Yositate Takane, “Generalized bulk-edge correspondence for non-hermitian topological systems,” *Physical Review B* **100**, 165430 (2019).
- [93] L Jin and Z Song, “Bulk-boundary correspondence in a non-hermitian system in one dimension with chiral inversion symmetry,” *Physical Review B* **99**, 081103 (2019).
- [94] Dan S. Borgnia, Alex Jura Kruchkov, and Robert-Jan Slager, “Non-hermitian boundary modes and topology,” *Phys. Rev. Lett.* **124**, 056802 (2020).
- [95] Linhu Li, Sen Mu, Ching Hua Lee, and Jiangbin Gong, “Quantized classical response from spectral winding topology,” *Nature communications* **12**, 5294 (2021).
- [96] Chenwei Lv, Ren Zhang, Zhengzheng Zhai, and Qi Zhou, “Curving the space by non-hermiticity,” *Nature communications* **13**, 2184 (2022).
- [97] Russell Yang, Jun Wei Tan, Tommy Tai, Jin Ming Koh, Linhu Li, Stefano Longhi, and Ching Hua Lee, “Designing non-hermitian real spectra through electrostatics,” *arXiv preprint arXiv:2201.04153* (2022).
- [98] Hui Jiang and Ching Hua Lee, “Dimensional transmutation from non-hermiticity,” (2022), [10.48550/ARXIV.2207.08843](https://arxiv.org/abs/10.48550/ARXIV.2207.08843).
- [99] Tommy Tai and Ching Hua Lee, “Zoology of non-hermitian spectra and their graph topology,” *arXiv preprint arXiv:2202.03462* (2022).
- [100] Ching Hua Lee, “Many-body topological and skin states without open boundaries,” *Physical Review B* **104**, 195102 (2021).
- [101] Ching Hua Lee, Linhu Li, Ronny Thomale, and Jiangbin Gong, “Unraveling non-hermitian pumping: Emergent spectral singularities and anomalous responses,” *Phys. Rev. B* **102**, 085151 (2020).
- [102] Linhu Li and Ching Hua Lee, “Non-hermitian pseudogaps,” *Science Bulletin* **67**, 685–690 (2022).
- [103] Ruizhe Shen and Ching Hua Lee, “Non-hermitian skin clusters from strong interactions,” *Communications Physics* **5**, 238 (2022).
- [104] Fang Qin, Ruizhe Shen, and Ching Hua Lee, “Non-hermitian squeezed polarons,” *Phys. Rev. A* **107**, L010202 (2023).
- [105] Ching Hua Lee, Linhu Li, and Jiangbin Gong, “Hybrid higher-order skin-topological modes in nonreciprocal systems,” *Physical review letters* **123**, 016805 (2019).
- [106] Kohei Kawabata, Nobuyuki Okuma, and Masatoshi Sato, “Non-bloch band theory of non-hermitian hamiltonians in the symplectic class,” *Phys. Rev. B* **101**, 195147 (2020).
- [107] Kazuki Yokomizo and Shuichi Murakami, “Non-bloch band theory and bulk–edge correspondence in non-hermitian systems,” *Progress of Theoretical and Experimental Physics* **2020**, 12A102 (2020).
- [108] Yifei Yi and Zhesen Yang, “Non-hermitian skin modes induced by on-site dissipations and chiral tunneling effect,” *Phys. Rev. Lett.* **125**, 186802 (2020).
- [109] Kazuki Yokomizo and Shuichi Murakami, “Topological semimetal phase with exceptional points in one-dimensional non-hermitian systems,” *Phys. Rev. Research* **2**, 043045 (2020).
- [110] Zhesen Yang, Kai Zhang, Chen Fang, and Jiangping Hu, “Non-hermitian bulk-boundary correspondence and auxiliary generalized brillouin zone theory,” *Phys. Rev. Lett.* **125**, 226402 (2020).
- [111] Kazuki Yokomizo and Shuichi Murakami, “Non-bloch band theory in bosonic bogoliubov–de gennes systems,” *Phys. Rev. B* **103**, 165123 (2021).
- [112] Tian-Shu Deng and Wei Yi, “Non-bloch topological invariants in a non-hermitian domain wall system,” *Phys. Rev. B* **100**, 035102 (2019).
- [113] Linhu Li, Ching Hua Lee, Sen Mu, and Jiangbin Gong, “Critical non-hermitian skin effect,” *Nature communications* **11**, 5491 (2020).
- [114] SM Rafi-UI-Islam, Zhuo Bin Siu, Haydar Sahin, Ching Hua Lee, and Mansoor BA Jalil, “Critical hybridization of skin modes in coupled non-hermitian chains,” *Physical Review Research* **4**, 013243 (2022).
- [115] Chun-Hui Liu, Kai Zhang, Zhesen Yang, and Shu Chen, “Helical damping and dynamical critical skin effect in open quantum systems,” *Physical Review Research* **2**, 043167 (2020).
- [116] SM Rafi-UI-Islam, Zhuo Bin Siu, Haydar Sahin, Ching Hua Lee, and Mansoor BA Jalil, “System size dependent topological zero modes in coupled topoelectrical chains,” *Physical Review B* **106**, 075158 (2022).
- [117] Pasquale Calabrese and John Cardy, “Entanglement entropy and conformal field theory,” *Journal of physics a: mathematical and theoretical* **42**, 504005 (2009).
- [118] Tatsuma Nishioka, Shinsei Ryu, and Tadashi Takayanagi, “Holographic entanglement entropy: an overview,” *Journal of Physics A: Mathematical and Theoretical* **42**, 504008 (2009).
- [119] Brian Swingle, “Entanglement renormalization and holography,” *Physical Review D* **86**, 065007 (2012).
- [120] Ching Hua Lee and Peng Ye, “Free-fermion entanglement spectrum through wannier interpolation,” *Physical Review B* **91**, 085119 (2015).
- [121] Yingfei Gu, Ching Hua Lee, Xueda Wen, Gil Young Cho, Shinsei Ryu, and Xiao-Liang Qi, “Holographic duality between (2+ 1)-dimensional quantum anomalous hall state and (3+ 1)-dimensional topological insulators,” *Physical Review B* **94**, 125107 (2016).
- [122] Loïc Herviou, Nicolas Regnault, and Jens H Bardarson, “Entanglement spectrum and symmetries in non-hermitian fermionic non-interacting models,” *SciPost Physics* **7**, 069 (2019).
- [123] Carlos Ortega-Taberner, Lukas Rødland, and Maria Hermanns, “Polarization and entanglement spectrum in non-hermitian systems,” *Physical Review B* **105**, 075103 (2022).
- [124] Nobuyuki Okuma and Masatoshi Sato, “Quantum anomaly, non-hermitian skin effects, and entanglement entropy in open systems,” *Physical Review B* **103**, 085428 (2021).
- [125] Li-Mei Chen, Yao Zhou, Shuai A Chen, and Peng Ye, “Quantum entanglement of non-hermitian quasicrystals,” *Physical Review B* **105**, L121115 (2022).
- [126] Kohei Kawabata, Tokiro Numasawa, and Shinsei Ryu, “Entanglement phase transition induced by the non-hermitian skin effect,” *arXiv preprint arXiv:2206.05384* (2022).
- [127] Kazuki Yokomizo and Shuichi Murakami, “Scaling rule for the critical non-hermitian skin effect,” *Phys. Rev. B* **104**, 165117 (2021).
- [128] LC Xie, Liang Jin, and Zhi Song, “Antihelical edge states in two-dimensional photonic topological metals,”

- Science Bulletin **68**, 255 (2023).
- [129] Midya Parto, Yuzhou GN Liu, Babak Bahari, Mercedeh Khajavikhan, and Demetrios N Christodoulides, “Non-hermitian and topological photonics: optics at an exceptional point,” *Nanophotonics* **10**, 403–423 (2020).
  - [130] Ramy El-Ganainy, Mercedeh Khajavikhan, Demetrios N Christodoulides, and Sahin K Ozdemir, “The dawn of non-hermitian optics,” *Communications Physics* **2**, 37 (2019).
  - [131] Bikashkali Midya, Han Zhao, and Liang Feng, “Non-hermitian photonics promises exceptional topology of light,” *Nature communications* **9**, 2674 (2018).
  - [132] Hongfei Wang, Biye Xie, Samit Kumar Gupta, Xueyi Zhu, Li Liu, Xiaoping Liu, Minghui Lu, and Yanfeng Chen, “Exceptional concentric rings in a non-hermitian bilayer photonic system,” *Physical Review B* **100**, 165134 (2019).
  - [133] Hongfei Wang, Xiujuan Zhang, Jinguo Hua, Dangyuan Lei, Minghui Lu, and Yanfeng Chen, “Topological physics of non-hermitian optics and photonics: a review,” *Journal of Optics* **23**, 123001 (2021).
  - [134] Martino De Carlo, Francesco De Leonardis, Richard A Soref, Luigi Colatorti, and Vittorio MN Passaro, “Non-hermitian sensing in photonics and electronics: A review,” *Sensors* **22**, 3977 (2022).
  - [135] Mohammad Hafezi, Sunil Mittal, J Fan, A Migdall, and JM Taylor, “Imaging topological edge states in silicon photonics,” *Nature Photonics* **7**, 1001–1005 (2013).
  - [136] Sunil Mittal, Venkata Vikram Orre, Guanyu Zhu, Maxim A Gorchach, Alexander Poddubny, and Mohammad Hafezi, “Photonic quadrupole topological phases,” *Nature Photonics* **13**, 692–696 (2019).
  - [137] This double degeneracy in  $\text{Im}(k)$  is required for the state to vanish at two boundaries that are arbitrary far apart.
  - [138] Kai Zhang, Zhesen Yang, and Chen Fang, “Correspondence between winding numbers and skin modes in non-hermitian systems,” *Physical Review Letters* **125**, 126402 (2020).
  - [139] Thus directed amplification provides an alternative mechanism for achieving real non-Hermitian spectra [97, 153], unrelated to PT symmetry.
  - [140] Ching Hua Lee and Stefano Longhi, “Ultrafast and anharmonic rabi oscillations between non-bloch bands,” *Communications Physics* **3**, 1–9 (2020).
  - [141] Although the GBZ also depends on the model, at least it remains invariant across models related by conformal transforms in the complex  $E_{\text{OBC}}$  plane [99, 101].
  - [142] Ching Hua Lee and Xiao-Liang Qi, “Lattice construction of pseudopotential hamiltonians for fractional chern insulators,” *Physical Review B* **90**, 085103 (2014).
  - [143] W. P. Su, J. R. Schrieffer, and A. J. Heeger, “Solitons in polyacetylene,” *Phys. Rev. Lett.* **42**, 1698–1701 (1979).
  - [144] Marcos Atala, Monika Aidelsburger, Julio T Barreiro, Dmitry Abanin, Takuya Kitagawa, Eugene Demler, and Immanuel Bloch, “Direct measurement of the zak phase in topological bloch bands,” *Nature Physics* **9**, 795–800 (2013).
  - [145] Lei Wang, Matthias Troyer, and Xi Dai, “Topological charge pumping in a one-dimensional optical lattice,” *Physical review letters* **111**, 026802 (2013).
  - [146] Michael Lohse, Christian Schweizer, Oded Zilberberg, Monika Aidelsburger, and Immanuel Bloch, “A thouless quantum pump with ultracold bosonic atoms in an optical superlattice,” *Nature Physics* **12**, 350–354 (2016).
  - [147] Shuta Nakajima, Takafumi Tomita, Shintaro Taie, Tomohiro Ichinose, Hideki Ozawa, Lei Wang, Matthias Troyer, and Yoshiro Takahashi, “Topological thouless pumping of ultracold fermions,” *Nature Physics* **12**, 296–300 (2016).
  - [148] Martin Leder, Christopher Grossert, Lukas Sitta, Maximilian Genske, Achim Rosch, and Martin Weitz, “Real-space imaging of a topologically protected edge state with ultracold atoms in an amplitude-chirped optical lattice,” *Nature communications* **7**, 13112 (2016).
  - [149] Linhu Li, Ching Hua Lee, and Jiangbin Gong, “Impurity induced scale-free localization,” *Communications Physics* **4**, 42 (2021).
  - [150] Motohiko Ezawa, “Dynamical nonlinear higher-order non-hermitian skin effects and topological trap-skin phase,” *Physical Review B* **105**, 125421 (2022).
  - [151] Hui Jiang and Ching Hua Lee, “Filling up complex spectral regions through non-hermitian disordered chains,” *Chinese Physics B* **31**, 050307 (2022).
  - [152] Cui-Xian Guo, Chun-Hui Liu, Xiao-Ming Zhao, Yanxia Liu, and Shu Chen, “Exact solution of non-hermitian systems with generalized boundary conditions: Size-dependent boundary effect and fragility of the skin effect,” *Physical Review Letters* **127**, 116801 (2021).
  - [153] Boxue Zhang, Qingya Li, Xiao Zhang, and Ching Hua Lee, “Real non-hermitian energy spectra without any symmetry,” *Chinese Physics B* **31**, 070308 (2022).



**Appendix A: Derivation of the determinant form of the OBC constraints for a two-band cNHSE model**  
[Eq. (8)]

From the bulk eigenequation in Eq. (6), we obtain:

$$\begin{cases} \left[ \sum_{n=-n_-}^{n_+} h_n^{aa} (\beta_j)^n - E_{\text{OBC}} \right] \phi_A^{(j)} + \sum_{n=-n_-}^{n_+} h_n^{ab} (\beta_j)^n \phi_B^{(j)} = 0, & \frac{\phi_B^{(j)}}{\phi_A^{(j)}} = \frac{E_{\text{OBC}} - \sum_{n=-n_-}^{n_+} h_n^{aa} (\beta_j)^n}{\sum_{n=-n_-}^{n_+} h_n^{ab} (\beta_j)^n}, \\ \sum_{n=-n_-}^{n_+} h_n^{ba} (\beta_j)^n \phi_A^{(j)} + \left[ \sum_{n=-n_-}^{n_+} h_n^{bb} (\beta_j)^n - E_{\text{OBC}} \right] \phi_B^{(j)} = 0, & \frac{\phi_B^{(j)}}{\phi_A^{(j)}} = \frac{\sum_{n=-n_-}^{n_+} h_n^{ba} (\beta_j)^n}{E_{\text{OBC}} - \sum_{n=-n_-}^{n_+} h_n^{bb} (\beta_j)^n}, \end{cases} \quad (\text{A1})$$

i.e.,

$$\frac{\phi_B^{(j)}}{\phi_A^{(j)}} = \frac{E_{\text{OBC}} - \sum_{n=-n_-}^{n_+} h_n^{aa} (\beta_j)^n}{\sum_{n=-n_-}^{n_+} h_n^{ab} (\beta_j)^n} = \frac{\sum_{n=-n_-}^{n_+} h_n^{ba} (\beta_j)^n}{E_{\text{OBC}} - \sum_{n=-n_-}^{n_+} h_n^{bb} (\beta_j)^n} = f_j, \quad (\text{A2})$$

$$\left[ \sum_{n=-n_-}^{n_+} h_n^{ab} (\beta_j)^n \right] \left[ \sum_{n=-n_-}^{n_+} h_n^{ba} (\beta_j)^n \right] = \left[ E_{\text{OBC}} - \sum_{n=-n_-}^{n_+} h_n^{aa} (\beta_j)^n \right] \left[ E_{\text{OBC}} - \sum_{n=-n_-}^{n_+} h_n^{bb} (\beta_j)^n \right] \quad (\text{A3})$$

$$\phi_B^{(j)} = f_j \phi_A^{(j)}. \quad (\text{A4})$$

which also relates  $E_{\text{OBC}}$  with  $\beta_j$  solutions.

Substituting these real-space eigenequations under the OBC constraints  $\psi_{-n_-, \alpha} = \dots = \psi_{-1, \alpha} = \psi_{0, \alpha} = \psi_{L+1, \alpha} = \psi_{L+2, \alpha} = \dots = \psi_{L+n_+, \alpha} = 0$  ( $\alpha = \text{A, B}$ ;  $1 \leq n_{\pm} \leq L/2$ ) into the real-space Schrödinger equation  $\mathcal{H}_{gr}|\psi\rangle = E_{\text{OBC}}|\psi\rangle$  [where  $\mathcal{H}_{gr}$  is the Hamiltonian matrix of  $H_{gr}$  in the basis  $(C_1, C_2, \dots, C_L)^T$ ], we can get

$$\left\{ \begin{array}{l} \sum_{n=0}^{n_+} h_n^{aa} \psi_{1+n, \text{A}} + \sum_{n=0}^{n_+} h_n^{ab} \psi_{1+n, \text{B}} = E_{\text{OBC}} \psi_{1, \text{A}}, \\ \sum_{n=0}^{n_+} h_n^{ba} \psi_{1+n, \text{A}} + \sum_{n=0}^{n_+} h_n^{bb} \psi_{1+n, \text{B}} = E_{\text{OBC}} \psi_{1, \text{B}}, \\ \sum_{n=-1}^{n_+} h_n^{aa} \psi_{2+n, \text{A}} + \sum_{n=-1}^{n_+} h_n^{ab} \psi_{2+n, \text{B}} = E_{\text{OBC}} \psi_{2, \text{A}}, \\ \sum_{n=-1}^{n_+} h_n^{ba} \psi_{2+n, \text{A}} + \sum_{n=-1}^{n_+} h_n^{bb} \psi_{2+n, \text{B}} = E_{\text{OBC}} \psi_{2, \text{B}}, \\ \vdots \\ \sum_{n=-(n_+-1)}^{n_+} h_n^{aa} \psi_{n_++n, \text{A}} + \sum_{n=-(n_+-1)}^{n_+} h_n^{ab} \psi_{n_++n, \text{B}} = E_{\text{OBC}} \psi_{n_+, \text{A}}, \quad 1 \leq 2n_+ \leq L, \quad 1 \leq n_+ \leq L/2, \\ \sum_{n=-(n_+-1)}^{n_+} h_n^{ba} \psi_{n_++n, \text{A}} + \sum_{n=-(n_+-1)}^{n_+} h_n^{bb} \psi_{n_++n, \text{B}} = E_{\text{OBC}} \psi_{n_+, \text{B}}, \quad 1 \leq 2n_+ \leq L, \quad 1 \leq n_+ \leq L/2, \\ \sum_{n=-n_-}^{n_+} h_n^{aa} \psi_{L-(n_+-1)+n, \text{A}} + \sum_{n=-n_-}^{n_+} h_n^{ab} \psi_{L-(n_+-1)+n, \text{B}} = E_{\text{OBC}} \psi_{L-(n_+-1), \text{A}}, \quad 1 \leq L-2n_++1 \leq L, \\ \sum_{n=-n_-}^{n_+} h_n^{ba} \psi_{L-(n_+-1)+n, \text{A}} + \sum_{n=-n_-}^{n_+} h_n^{bb} \psi_{L-(n_+-1)+n, \text{B}} = E_{\text{OBC}} \psi_{L-(n_+-1), \text{B}}, \quad 1 \leq n_- \leq L/2, \\ \vdots \\ \sum_{n=-n_-}^1 h_n^{aa} \psi_{L-1+n, \text{A}} + \sum_{n=-n_-}^1 h_n^{ab} \psi_{L-1+n, \text{B}} = E_{\text{OBC}} \psi_{L-1, \text{A}}, \\ \sum_{n=-n_-}^1 h_n^{ba} \psi_{L-1+n, \text{A}} + \sum_{n=-n_-}^1 h_n^{bb} \psi_{L-1+n, \text{B}} = E_{\text{OBC}} \psi_{L-1, \text{B}}, \\ \sum_{n=-n_-}^0 h_n^{aa} \psi_{L+n, \text{A}} + \sum_{n=-n_-}^0 h_n^{ab} \psi_{L+n, \text{B}} = E_{\text{OBC}} \psi_{L, \text{A}}, \quad 1 \leq L-n_- \leq L, \quad 0 \leq n_- \leq L-1, \\ \sum_{n=-n_-}^0 h_n^{ba} \psi_{L+n, \text{A}} + \sum_{n=-n_-}^0 h_n^{bb} \psi_{L+n, \text{B}} = E_{\text{OBC}} \psi_{L, \text{B}}, \quad 1 \leq L-n_- \leq L, \quad 0 \leq n_- \leq L-1. \end{array} \right. \quad (\text{A5})$$

Invoking the non-Bloch ansatz  $(\psi_{n, \text{A}}, \psi_{n, \text{B}})^T = \sum_{j=1}^{2M} (\beta_j)^n \left( \phi_A^{(j)}, \phi_B^{(j)} \right)^T$  ( $M = n_- + n_+$ ) into the above equations

(A5), we have, generalizing [89],

$$\left\{ \begin{array}{l}
 \sum_{j=1}^{2M} \sum_{n=0}^{n_+} h_n^{aa} (\beta_j)^{1+n} \phi_A^{(j)} + \sum_{j=1}^{2M} \sum_{n=0}^{n_+} h_n^{ab} (\beta_j)^{1+n} \phi_B^{(j)} = E_{\text{OBC}} \sum_{j=1}^{2M} (\beta_j) \phi_A^{(j)}, \\
 \sum_{j=1}^{2M} \sum_{n=0}^{n_+} h_n^{ba} (\beta_j)^{1+n} \phi_A^{(j)} + \sum_{j=1}^{2M} \sum_{n=0}^{n_+} h_n^{bb} (\beta_j)^{1+n} \phi_B^{(j)} = E_{\text{OBC}} \sum_{j=1}^{2M} (\beta_j) \phi_B^{(j)}, \\
 \sum_{j=1}^{2M} \sum_{n=-1}^{n_+} h_n^{aa} (\beta_j)^{2+n} \phi_A^{(j)} + \sum_{j=1}^{2M} \sum_{n=-1}^{n_+} h_n^{ab} (\beta_j)^{2+n} \phi_B^{(j)} = E_{\text{OBC}} \sum_{j=1}^{2M} (\beta_j)^2 \phi_A^{(j)}, \\
 \sum_{j=1}^{2M} \sum_{n=-1}^{n_+} h_n^{ba} (\beta_j)^{2+n} \phi_A^{(j)} + \sum_{j=1}^{2M} \sum_{n=-1}^{n_+} h_n^{bb} (\beta_j)^{2+n} \phi_B^{(j)} = E_{\text{OBC}} \sum_{j=1}^{2M} (\beta_j)^2 \phi_B^{(j)}, \\
 \vdots \\
 \sum_{j=1}^{2M} \sum_{n=-(n_+-1)}^{n_+} h_n^{aa} (\beta_j)^{n_++n} \phi_A^{(j)} + \sum_{j=1}^{2M} \sum_{n=-(n_+-1)}^{n_+} h_n^{ab} (\beta_j)^{n_++n} \phi_B^{(j)} = E_{\text{OBC}} \sum_{j=1}^{2M} (\beta_j)^{n_+} \phi_A^{(j)}, \\
 \sum_{j=1}^{2M} \sum_{n=-(n_+-1)}^{n_+} h_n^{ba} (\beta_j)^{n_++n} \phi_A^{(j)} + \sum_{j=1}^{2M} \sum_{n=-(n_+-1)}^{n_+} h_n^{bb} (\beta_j)^{n_++n} \phi_B^{(j)} = E_{\text{OBC}} \sum_{j=1}^{2M} (\beta_j)^{n_+} \phi_B^{(j)}, \\
 \sum_{j=1}^{2M} \sum_{n=-n_-}^{n_+-1} h_n^{aa} (\beta_j)^{L-(n_+-1)+n} \phi_A^{(j)} + \sum_{j=1}^{2M} \sum_{n=-n_-}^{n_+-1} h_n^{ab} (\beta_j)^{L-(n_+-1)+n} \phi_B^{(j)} = E_{\text{OBC}} \sum_{j=1}^{2M} (\beta_j)^{L-(n_+-1)} \phi_A^{(j)}, \\
 \sum_{j=1}^{2M} \sum_{n=-n_-}^{n_+-1} h_n^{ba} (\beta_j)^{L-(n_+-1)+n} \phi_A^{(j)} + \sum_{j=1}^{2M} \sum_{n=-n_-}^{n_+-1} h_n^{bb} (\beta_j)^{L-(n_+-1)+n} \phi_B^{(j)} = E_{\text{OBC}} \sum_{j=1}^{2M} (\beta_j)^{L-(n_+-1)} \phi_B^{(j)}, \\
 \vdots \\
 \sum_{j=1}^{2M} \sum_{n=-n_-}^1 h_n^{aa} (\beta_j)^{L-1+n} \phi_A^{(j)} + \sum_{j=1}^{2M} \sum_{n=-n_-}^1 h_n^{ab} (\beta_j)^{L-1+n} \phi_B^{(j)} = E_{\text{OBC}} \sum_{j=1}^{2M} (\beta_j)^{L-1} \phi_A^{(j)}, \\
 \sum_{j=1}^{2M} \sum_{n=-n_-}^1 h_n^{ba} (\beta_j)^{L-1+n} \phi_A^{(j)} + \sum_{j=1}^{2M} \sum_{n=-n_-}^1 h_n^{bb} (\beta_j)^{L-1+n} \phi_B^{(j)} = E_{\text{OBC}} \sum_{j=1}^{2M} (\beta_j)^{L-1} \phi_B^{(j)}, \\
 \sum_{j=1}^{2M} \sum_{n=-n_-}^0 h_n^{aa} (\beta_j)^{L+n} \phi_A^{(j)} + \sum_{j=1}^{2M} \sum_{n=-n_-}^0 h_n^{ab} (\beta_j)^{L+n} \phi_B^{(j)} = E_{\text{OBC}} \sum_{j=1}^{2M} (\beta_j)^L \phi_A^{(j)}, \\
 \sum_{j=1}^{2M} \sum_{n=-n_-}^0 h_n^{ba} (\beta_j)^{L+n} \phi_A^{(j)} + \sum_{j=1}^{2M} \sum_{n=-n_-}^0 h_n^{bb} (\beta_j)^{L+n} \phi_B^{(j)} = E_{\text{OBC}} \sum_{j=1}^{2M} (\beta_j)^L \phi_B^{(j)}.
 \end{array} \right. \quad (\text{A6})$$

Substituting Eq. (A4), i.e.,  $\phi_B^{(j)} = f_j \phi_A^{(j)}$  into the above equations (A6) such as to eliminate the  $\phi_B^{(j)}$ , we have

$$\left\{ \begin{array}{l}
 \sum_{j=1}^{2M} [\sum_{n=0}^{n_+} (h_n^{aa} + f_j h_n^{ab}) (\beta_j)^n - E_{\text{OBC}}] (\beta_j) \phi_A^{(j)} = 0, \\
 \sum_{j=1}^{2M} [\sum_{n=0}^{n_+} (h_n^{ba} + f_j h_n^{bb}) (\beta_j)^n - f_j E_{\text{OBC}}] (\beta_j) \phi_A^{(j)} = 0, \\
 \sum_{j=1}^{2M} [\sum_{n=-1}^{n_+} (h_n^{aa} + f_j h_n^{ab}) (\beta_j)^n - E_{\text{OBC}}] (\beta_j)^2 \phi_A^{(j)} = 0, \\
 \sum_{j=1}^{2M} [\sum_{n=-1}^{n_+} (h_n^{ba} + f_j h_n^{bb}) (\beta_j)^n - f_j E_{\text{OBC}}] (\beta_j)^2 \phi_A^{(j)} = 0, \\
 \vdots \\
 \sum_{j=1}^{2M} [\sum_{n=-(n_+-1)}^{n_+} (h_n^{aa} + f_j h_n^{ab}) (\beta_j)^n - E_{\text{OBC}}] (\beta_j)^{n_+} \phi_A^{(j)} = 0, \\
 \sum_{j=1}^{2M} [\sum_{n=-(n_+-1)}^{n_+} (h_n^{ba} + f_j h_n^{bb}) (\beta_j)^n - f_j E_{\text{OBC}}] (\beta_j)^{n_+} \phi_A^{(j)} = 0, \\
 \sum_{j=1}^{2M} [\sum_{n=-n_-}^{n_+-1} (h_n^{aa} + f_j h_n^{ab}) (\beta_j)^n - E_{\text{OBC}}] (\beta_j)^{L-(n_+-1)} \phi_A^{(j)} = 0, \\
 \sum_{j=1}^{2M} [\sum_{n=-n_-}^{n_+-1} (h_n^{ba} + f_j h_n^{bb}) (\beta_j)^n - f_j E_{\text{OBC}}] (\beta_j)^{L-(n_+-1)} \phi_A^{(j)} = 0, \\
 \vdots \\
 \sum_{j=1}^{2M} [\sum_{n=-n_-}^1 (h_n^{aa} + f_j h_n^{ab}) (\beta_j)^n - E_{\text{OBC}}] (\beta_j)^{L-1} \phi_A^{(j)} = 0, \\
 \sum_{j=1}^{2M} [\sum_{n=-n_-}^1 (h_n^{ba} + f_j h_n^{bb}) (\beta_j)^n - f_j E_{\text{OBC}}] (\beta_j)^{L-1} \phi_A^{(j)} = 0, \\
 \sum_{j=1}^{2M} [\sum_{n=-n_-}^0 (h_n^{aa} + f_j h_n^{ab}) (\beta_j)^n - E_{\text{OBC}}] (\beta_j)^L \phi_A^{(j)} = 0, \\
 \sum_{j=1}^{2M} [\sum_{n=-n_-}^0 (h_n^{ba} + f_j h_n^{bb}) (\beta_j)^n - f_j E_{\text{OBC}}] (\beta_j)^L \phi_A^{(j)} = 0.
 \end{array} \right. \quad (\text{A7})$$

We can express Eq. (A7) in more compact notation

$$\left\{ \begin{array}{l} \sum_{j=1}^{2M} F_j^{(a,1)} \beta_j \phi_A^{(j)} = 0, \\ \sum_{j=1}^{2M} F_j^{(b,1)} \beta_j \phi_A^{(j)} = 0, \\ \vdots \\ \sum_{j=1}^{2M} F_j^{(a,n_+)} (\beta_j)^{n_+} \phi_A^{(j)} = 0, \\ \sum_{j=1}^{2M} F_j^{(b,n_+)} (\beta_j)^{n_+} \phi_A^{(j)} = 0, \\ \sum_{j=1}^{2M} G_j^{(a,1)} (\beta_j)^{L-(n_+-1)} \phi_A^{(j)} = 0, \\ \sum_{j=1}^{2M} G_j^{(b,1)} (\beta_j)^{L-(n_+-1)} \phi_A^{(j)} = 0, \\ \vdots \\ \sum_{j=1}^{2M} G_j^{(a,n_-)} (\beta_j)^L \phi_A^{(j)} = 0, \\ \sum_{j=1}^{2M} G_j^{(b,n_-)} (\beta_j)^L \phi_A^{(j)} = 0, \end{array} \right. \quad (\text{A8})$$

where

$$F_j^{(a,i)} = \sum_{n=-(i-1)}^{n_+} (h_n^{aa} + f_j h_n^{ab}) (\beta_j)^n - E_{\text{OBC}}, \quad (\text{A9})$$

$$F_j^{(b,i)} = \sum_{n=-(i-1)}^{n_+} (h_n^{ba} + f_j h_n^{bb}) (\beta_j)^n - f_j E_{\text{OBC}}, \quad (\text{A10})$$

$$G_j^{(a,i)} = \sum_{n=-n_-}^{n_+-i} (h_n^{aa} + f_j h_n^{ab}) (\beta_j)^n - E_{\text{OBC}}, \quad (\text{A11})$$

$$G_j^{(b,i)} = \sum_{n=-n_-}^{n_+-i} (h_n^{ba} + f_j h_n^{bb}) (\beta_j)^n - f_j E_{\text{OBC}}. \quad (\text{A12})$$

For a nontrivial state  $\phi_A^{(j)}$  ( $j = 1, 2, \dots, 2M$ ) that does not vanish, we hence require the vanishing determinant

$$\begin{vmatrix} F_1^{(a,1)} \beta_1 & F_2^{(a,1)} \beta_2 & \cdots & F_{2M}^{(a,1)} \beta_{2M} \\ F_1^{(b,1)} \beta_1 & F_2^{(b,1)} \beta_2 & \cdots & F_{2M}^{(b,1)} \beta_{2M} \\ \vdots & \vdots & \vdots & \vdots \\ F_1^{(a,n_+)} (\beta_1)^{n_+} & F_2^{(a,n_+)} (\beta_2)^{n_+} & \cdots & F_{2M}^{(a,n_+)} (\beta_{2M})^{n_+} \\ F_1^{(b,n_+)} (\beta_1)^{n_+} & F_2^{(b,n_+)} (\beta_2)^{n_+} & \cdots & F_{2M}^{(b,n_+)} (\beta_{2M})^{n_+} \\ G_1^{(a,1)} (\beta_1)^{L-(n_+-1)} & G_2^{(a,1)} (\beta_2)^{L-(n_+-1)} & \cdots & G_{2M}^{(a,1)} (\beta_{2M})^{L-(n_+-1)} \\ G_1^{(b,1)} (\beta_1)^{L-(n_+-1)} & G_2^{(b,1)} (\beta_2)^{L-(n_+-1)} & \cdots & G_{2M}^{(b,1)} (\beta_{2M})^{L-(n_+-1)} \\ \vdots & \vdots & \vdots & \vdots \\ G_1^{(a,n_-)} (\beta_1)^L & G_2^{(a,n_-)} (\beta_2)^L & \cdots & G_{2M}^{(a,n_-)} (\beta_{2M})^L \\ G_1^{(b,n_-)} (\beta_1)^L & G_2^{(b,n_-)} (\beta_2)^L & \cdots & G_{2M}^{(b,n_-)} (\beta_{2M})^L \end{vmatrix} = 0. \quad (\text{A13})$$

## Appendix B: Derivation of the determinant form of the OBC constraints for a general multi-band model

Here, we generalize the above derivation to a general multi-band model, and show that the OBC constraints result in an analogous vanishing determinant expression. In momentum space, an  $N$ -band model Hamiltonian in the basis  $C_{\mathbf{k}} = (c_{\mathbf{k},1}, c_{\mathbf{k},2}, \dots, c_{\mathbf{k},N})^T$  is given by

$$\mathcal{H}_{mb}(z) = \sum_{n=-n_-}^{n_+} \begin{pmatrix} h_n^{11} & h_n^{12} & \cdots & h_n^{1N} \\ h_n^{21} & h_n^{22} & \cdots & h_n^{2N} \\ \vdots & \vdots & \vdots & \vdots \\ h_n^{N1} & h_n^{N2} & \cdots & h_n^{NN} \end{pmatrix} z^n, \quad (\text{B1})$$

where  $N$  is the number of bands, which we set to be an even number.

By Fourier transformation, one obtains the real-space tight-binding Hamiltonian of this system as

$$H_{mbr} = \sum_{j=1}^L \sum_{n=-n_-}^{n_+} C_j^\dagger \begin{pmatrix} h_n^{11} & h_n^{12} & \cdots & h_n^{1N} \\ h_n^{21} & h_n^{22} & \cdots & h_n^{2N} \\ \vdots & \vdots & \ddots & \vdots \\ h_n^{N1} & h_n^{N2} & \cdots & h_n^{NN} \end{pmatrix} C_{j+n}, \quad (\text{B2})$$

where  $C_j = (c_{j,1}, c_{j,2}, \dots, c_{j,N})^T$ .

With  $|\psi\rangle = (\psi_{1,1}, \psi_{1,2}, \dots, \psi_{1,N}, \psi_{2,1}, \psi_{2,2}, \dots, \psi_{2,N}, \dots, \psi_{L,1}, \psi_{L,2}, \dots, \psi_{L,N})^T$ , the solutions of the real-space Schrödinger equation  $\mathcal{H}_{mbr}|\psi\rangle = E_{\text{OBC}}|\psi\rangle$  [where  $\mathcal{H}_{mbr}$  is the Hamiltonian matrix of  $H_{mbr}$  in the basis  $(C_1, C_2, \dots, C_L)^T$ ] can be given by

$$\begin{pmatrix} \psi_{n,1} \\ \psi_{n,2} \\ \vdots \\ \psi_{n,N} \end{pmatrix} = \sum_{j=1}^{2M} (\beta_j)^n \begin{pmatrix} \phi_1^{(j)} \\ \phi_2^{(j)} \\ \vdots \\ \phi_N^{(j)} \end{pmatrix}, \quad (\text{B3})$$

where  $2M = N \times (n_- + n_+)$  and  $\beta = \beta_j$  are the solutions of the characteristic equation

$$\text{Det}[\mathcal{H}_{mb}(\beta) - E_{\text{OBC}}] = 0, \quad (\text{B4})$$

where  $\mathcal{H}_{mb}(\beta)$  is the non-Bloch matrix [127] as

$$\mathcal{H}_{mb}(\beta) = \sum_{n=-n_-}^{n_+} \begin{pmatrix} h_n^{11} & h_n^{12} & \cdots & h_n^{1N} \\ h_n^{21} & h_n^{22} & \cdots & h_n^{2N} \\ \vdots & \vdots & \ddots & \vdots \\ h_n^{N1} & h_n^{N2} & \cdots & h_n^{NN} \end{pmatrix} \beta^n. \quad (\text{B5})$$

In general, the characteristic equation (B4) has  $2M$  solutions for  $\beta$ , where  $M = N \times (n_- + n_+)/2$  is an integer and  $N$  is an even number. We label these solutions such that  $|\beta_1| \leq |\beta_2| \leq \dots \leq |\beta_{2M}|$ .

From the eigenequations, we obtain

$$\begin{cases} \sum_{n=-n_-}^{n_+} h_n^{11} (\beta_j)^n \phi_1^{(j)} + \sum_{n=-n_-}^{n_+} h_n^{12} (\beta_j)^n \phi_2^{(j)} + \cdots + \sum_{n=-n_-}^{n_+} h_n^{1N} (\beta_j)^n \phi_N^{(j)} = E_{\text{OBC}} \phi_1^{(j)}, \\ \sum_{n=-n_-}^{n_+} h_n^{21} (\beta_j)^n \phi_1^{(j)} + \sum_{n=-n_-}^{n_+} h_n^{22} (\beta_j)^n \phi_2^{(j)} + \cdots + \sum_{n=-n_-}^{n_+} h_n^{2N} (\beta_j)^n \phi_N^{(j)} = E_{\text{OBC}} \phi_2^{(j)}, \\ \vdots \\ \sum_{n=-n_-}^{n_+} h_n^{N1} (\beta_j)^n \phi_1^{(j)} + \sum_{n=-n_-}^{n_+} h_n^{N2} (\beta_j)^n \phi_2^{(j)} + \cdots + \sum_{n=-n_-}^{n_+} h_n^{NN} (\beta_j)^n \phi_N^{(j)} = E_{\text{OBC}} \phi_N^{(j)}, \end{cases} \quad (\text{B6})$$

i.e.,

$$\begin{cases} \left[ \sum_{n=-n_-}^{n_+} h_n^{11} (\beta_j)^n - E_{\text{OBC}} \right] \phi_1^{(j)} + \sum_{n=-n_-}^{n_+} h_n^{12} (\beta_j)^n \phi_2^{(j)} + \cdots + \sum_{n=-n_-}^{n_+} h_n^{1N} (\beta_j)^n \phi_N^{(j)} = 0, \\ \sum_{n=-n_-}^{n_+} h_n^{21} (\beta_j)^n \phi_1^{(j)} + \left[ \sum_{n=-n_-}^{n_+} h_n^{22} (\beta_j)^n - E_{\text{OBC}} \right] \phi_2^{(j)} + \cdots + \sum_{n=-n_-}^{n_+} h_n^{2N} (\beta_j)^n \phi_N^{(j)} = 0, \\ \vdots \\ \sum_{n=-n_-}^{n_+} h_n^{N1} (\beta_j)^n \phi_1^{(j)} + \sum_{n=-n_-}^{n_+} h_n^{N2} (\beta_j)^n \phi_2^{(j)} + \cdots + \left[ \sum_{n=-n_-}^{n_+} h_n^{NN} (\beta_j)^n - E_{\text{OBC}} \right] \phi_N^{(j)} = 0, \end{cases} \quad (\text{B7})$$

i.e.,

$$\begin{cases} \left[ \sum_{n=-n_-}^{n_+} h_n^{11} (\beta_j)^n - E_{\text{OBC}} \right] \phi_1^{(j)} + \sum_{n=-n_-}^{n_+} h_n^{12} (\beta_j)^n f_j^{(2)} \phi_1^{(j)} + \cdots + \sum_{n=-n_-}^{n_+} h_n^{1N} (\beta_j)^n f_j^{(N)} \phi_1^{(j)} = 0, \\ \sum_{n=-n_-}^{n_+} h_n^{21} (\beta_j)^n \phi_1^{(j)} + \left[ \sum_{n=-n_-}^{n_+} h_n^{22} (\beta_j)^n - E_{\text{OBC}} \right] f_j^{(2)} \phi_1^{(j)} + \cdots + \sum_{n=-n_-}^{n_+} h_n^{2N} (\beta_j)^n f_j^{(N)} \phi_1^{(j)} = 0, \\ \vdots \\ \sum_{n=-n_-}^{n_+} h_n^{N1} (\beta_j)^n \phi_1^{(j)} + \sum_{n=-n_-}^{n_+} h_n^{N2} (\beta_j)^n f_j^{(2)} \phi_1^{(j)} + \cdots + \left[ \sum_{n=-n_-}^{n_+} h_n^{NN} (\beta_j)^n - E_{\text{OBC}} \right] f_j^{(N)} \phi_1^{(j)} = 0, \end{cases} \quad (\text{B8})$$

where  $f_j^{(\alpha)} = \phi_\alpha^{(j)} / \phi_1^{(j)}$  with  $\alpha = 1, 2, \dots, N$ , i.e.,

$$\phi_\alpha^{(j)} = f_j^{(\alpha)} \phi_1^{(j)}, \quad (\text{B9})$$



where  $\alpha = 1, 2, \dots, N$ .

As we know, Eq. (B3) has  $2M \times N$  unknown coefficients, but with the real-space Schrödinger equation  $\mathcal{H}_{mbr}|\psi\rangle = E_{\text{OBC}}|\psi\rangle$  and an additional  $2M$  boundary conditions, the  $2M \times N$  coefficients can be reduced to  $2M$ -independent coefficients. By rewriting the coupling constraints in terms of  $\phi_1^{(j)}$  ( $j = 1, 2, \dots, 2M$ ), which should have nonzero values, we have, analogously as before,

$$\begin{vmatrix} \tilde{F}_1^{(1,1)}\beta_1 & \tilde{F}_2^{(1,1)}\beta_2 & \cdots & \tilde{F}_{2M}^{(1,1)}\beta_{2M} \\ \tilde{F}_1^{(2,1)}\beta_1 & \tilde{F}_2^{(2,1)}\beta_2 & \cdots & \tilde{F}_{2M}^{(2,1)}\beta_{2M} \\ \vdots & \vdots & \vdots & \vdots \\ \tilde{F}_1^{(N,1)}\beta_1 & \tilde{F}_2^{(N,1)}\beta_2 & \cdots & \tilde{F}_{2M}^{(N,1)}\beta_{2M} \\ \vdots & \vdots & \vdots & \vdots \\ \tilde{F}_1^{(1,n_+)}(\beta_1)^{n_+} & \tilde{F}_2^{(1,n_+)}(\beta_2)^{n_+} & \cdots & \tilde{F}_{2M}^{(1,n_+)}(\beta_{2M})^{n_+} \\ \tilde{F}_1^{(2,n_+)}(\beta_1)^{n_+} & \tilde{F}_2^{(2,n_+)}(\beta_2)^{n_+} & \cdots & \tilde{F}_{2M}^{(2,n_+)}(\beta_{2M})^{n_+} \\ \vdots & \vdots & \vdots & \vdots \\ \tilde{F}_1^{(N,n_+)}(\beta_1)^{n_+} & \tilde{F}_2^{(N,n_+)}(\beta_2)^{n_+} & \cdots & \tilde{F}_{2M}^{(N,n_+)}(\beta_{2M})^{n_+} \\ \tilde{G}_1^{(1,1)}(\beta_1)^{L-(n_+-1)} & \tilde{G}_2^{(1,1)}(\beta_2)^{L-(n_+-1)} & \cdots & \tilde{G}_{2M}^{(1,1)}(\beta_{2M})^{L-(n_+-1)} \\ \tilde{G}_1^{(2,1)}(\beta_1)^{L-(n_+-1)} & \tilde{G}_2^{(2,1)}(\beta_2)^{L-(n_+-1)} & \cdots & \tilde{G}_{2M}^{(2,1)}(\beta_{2M})^{L-(n_+-1)} \\ \vdots & \vdots & \vdots & \vdots \\ \tilde{G}_1^{(N,1)}(\beta_1)^{L-(n_+-1)} & \tilde{G}_2^{(N,1)}(\beta_2)^{L-(n_+-1)} & \cdots & \tilde{G}_{2M}^{(N,1)}(\beta_{2M})^{L-(n_+-1)} \\ \vdots & \vdots & \vdots & \vdots \\ \tilde{G}_1^{(1,n_-)}(\beta_1)^L & \tilde{G}_2^{(1,n_-)}(\beta_2)^L & \cdots & \tilde{G}_{2M}^{(1,n_-)}(\beta_{2M})^L \\ \tilde{G}_1^{(2,n_-)}(\beta_1)^L & \tilde{G}_2^{(2,n_-)}(\beta_2)^L & \cdots & \tilde{G}_{2M}^{(2,n_-)}(\beta_{2M})^L \\ \vdots & \vdots & \vdots & \vdots \\ \tilde{G}_1^{(N,n_-)}(\beta_1)^L & \tilde{G}_2^{(N,n_-)}(\beta_2)^L & \cdots & \tilde{G}_{2M}^{(N,n_-)}(\beta_{2M})^L \end{vmatrix} = 0, \quad (\text{B10})$$

where

$$\tilde{F}_j^{(1,i)} = \sum_{n=-(i-1)}^{n_+} (h_n^{11} + f_j^{(2)}h_n^{12} + \cdots + f_j^{(N)}h_n^{1N})(\beta_j)^n - E_{\text{OBC}}, \quad (\text{B11})$$

$$\tilde{F}_j^{(2,i)} = \sum_{n=-(i-1)}^{n_+} (h_n^{21} + f_j^{(2)}h_n^{22} + \cdots + f_j^{(N)}h_n^{2N})(\beta_j)^n - f_j^{(2)}E_{\text{OBC}}, \quad (\text{B12})$$

$\vdots$

$$\tilde{F}_j^{(N,i)} = \sum_{n=-(i-1)}^{n_+} (h_n^{N1} + f_j^{(2)}h_n^{N2} + \cdots + f_j^{(N)}h_n^{NN})(\beta_j)^n - f_j^{(N)}E_{\text{OBC}}, \quad (\text{B13})$$

$$\tilde{G}_j^{(1,i)} = \sum_{n=-n_-}^{n_--i} (h_n^{11} + f_j^{(2)}h_n^{12} + \cdots + f_j^{(N)}h_n^{1N})(\beta_j)^n - E_{\text{OBC}}, \quad (\text{B14})$$

$$\tilde{G}_j^{(2,i)} = \sum_{n=-n_-}^{n_--i} (h_n^{12} + f_j^{(2)}h_n^{22} + \cdots + f_j^{(N)}h_n^{2N})(\beta_j)^n - f_j^{(2)}E_{\text{OBC}}, \quad (\text{B15})$$

$\vdots$

$$\tilde{G}_j^{(N,i)} = \sum_{n=-n_-}^{n_--i} (h_n^{N1} + f_j^{(2)}h_n^{N2} + \cdots + f_j^{(N)}h_n^{NN})(\beta_j)^n - f_j^{(N)}E_{\text{OBC}}. \quad (\text{B16})$$

We can collect the terms and express Eq. (B10) as a multivariate polynomial of the form

$$\sum_{P,Q} \tilde{J}(\beta_{i \in P}, \beta_{j \in Q}, E_{\text{OBC}}) \left[ \prod_{i \in P} (\beta_i)^k \right] \left[ \prod_{j \in Q} (\beta_j)^{k'} \right] = 0, \quad (\text{B17})$$

where  $k = 1, \dots, n_+$ ,  $k' = L - (n_- - 1), \dots, L$ , the sets  $P$  and  $Q$  are two disjoint subsets of the set  $\{1, 2, \dots, 2M\}$  with  $M$  elements, respectively.

By setting  $n_+ = n_-$ , Eq. (B17) can be reduced to

$$\sum_{P,Q} \tilde{J}(\beta_{i \in P}, \beta_{j \in Q}, E_{\text{OBC}}) \left[ \prod_{i \in P} (\beta_i)^{L+1} \right] = 0. \quad (\text{B18})$$

In Eq. (B18), there are two leading terms proportional to  $(\beta_M \beta_{M+2} \beta_{M+3} \dots \beta_{2M})^{L+1}$  and  $(\beta_{M+1} \beta_{M+2} \beta_{M+3} \dots \beta_{2M})^{L+1}$ . Therefore, in the limit of large system size  $L$ , we can reduce (B18), which solves the characteristic dispersion equation (B4) and open boundary conditions, to the familiar form

$$\left| \frac{\beta_M}{\beta_{M+1}} \right| \simeq \left| - \frac{\tilde{J}(\beta_{i \in P_1}, \beta_{j \in Q_1}, E_{\text{OBC}})}{\tilde{J}(\beta_{i \in P_2}, \beta_{j \in Q_2}, E_{\text{OBC}})} \right|_{E_{\text{OBC}}=E_\infty}^{\frac{1}{L+1}}, \quad (\text{B19})$$

where  $P_1 = \{M+1, M+2, M+3, \dots, 2M\}$ ,  $Q_1 = \{1, 2, 3, \dots, M\}$ ,  $P_2 = \{M, M+2, M+3, \dots, 2M\}$ ,  $Q_2 = \{1, 2, \dots, M-2, M-1, M+1\}$ , and  $L$  is the system size with  $L \rightarrow \infty$ . For large  $L$ , the right hand side (RHS) tends towards unity, and hence  $|\beta_M| \approx |\beta_{M+1}|$  for the OBC eigenfunctions in the thermodynamic limit (in practice,  $L \simeq 20$  is usually sufficient large when the cNHSE is *absent*).

### Appendix C: Numerical confirmation of the validity of the GBZ upon extrapolating to finite-size systems

Here in Fig. 12, we numerically confirm that for our coupled Hatano-Nelson model, the GBZ solutions  $\beta_M = \beta_2$  and  $\beta_{M+1} = \beta_3$  still largely determine the eigensolution decay rates down to small system sizes.

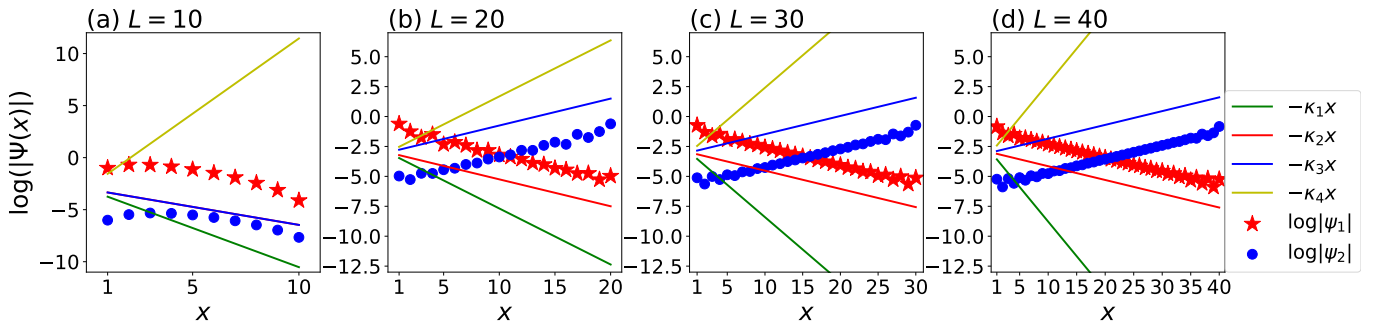


FIG. 12. Spatial decay of eigenstates and how they are determined by  $\beta_M$  and  $\beta_{M+1}$  ( $M = 2$ ). Plotted are the  $\log(|\psi(x)|)$  ( $\log(|\psi(x)|) = \ln(|\psi(x)|)$ ) of two representative eigenstates with different left/right localizations (red stars and blue disks), at different finite system sizes  $L = 10, 20, 30, 40$  (a)–(d). Compared against them are the decay profiles corresponding to the four  $\kappa = -\log |\beta| = -\ln |\beta|$  solutions. We see that  $|\beta_2| = e^{-\kappa_2}$  and  $|\beta_3| = e^{-\kappa_3}$  controls the eigenstate decay rate very well down to  $L = 20$ , even though in principle, they rigorously determine the decay rate only in the thermodynamic limit. (a) The eigenstates correspond to  $\arg(E_{\text{OBC}}) = 0$  and  $\text{Max}(\text{Re}(E_{\text{OBC}}))$ . (b)–(d) The eigenstates correspond to  $\arg(E_{\text{OBC}}) = \frac{\pi}{2}$ . Here,  $V = 0.5$  and the other parameters are  $t_0 = 0.01$ ,  $t_1 = 0.75$ , and  $\delta_a = -\delta_b = 0.25$ , which are the same as those in Fig. 1 of the main text.

### Appendix D: Derivation of Eq. (24) for the OBC constraints of the coupled Hatano-Nelson model

From the real-space eigenequations (20) subjected to OBCs  $\psi_{0,\alpha} = \psi_{L+1,\alpha} = 0$  ( $\alpha = A, B$ ), we have

$$\begin{cases} t_0 \psi_{1,B} + t_a^+ \psi_{2,A} + V \psi_{1,A} = E_{\text{OBC}} \psi_{1,A}, \\ t_0 \psi_{1,A} + t_b^+ \psi_{2,B} - V \psi_{1,B} = E_{\text{OBC}} \psi_{1,B}, \\ t_a^- \psi_{L-1,A} + t_0 \psi_{L,B} + V \psi_{L,A} = E_{\text{OBC}} \psi_{L,A}, \\ t_b^- \psi_{L-1,B} + t_0 \psi_{L,A} - V \psi_{L,B} = E_{\text{OBC}} \psi_{L,B}. \end{cases} \quad (\text{D1})$$

By substituting the ansatz  $(\psi_{n,A}, \psi_{n,B})^T = \sum_{j=1}^4 \beta_j^n \left( \phi_A^{(j)}, \phi_B^{(j)} \right)^T$  into Eq. (D1), we can get

$$\begin{cases} t_0 \sum_{j=1}^4 \beta_j \phi_B^{(j)} + t_a^+ \sum_{j=1}^4 \beta_j^2 \phi_A^{(j)} + V \sum_{j=1}^4 \beta_j \phi_A^{(j)} = E_{\text{OBC}} \sum_{j=1}^4 \beta_j \phi_A^{(j)}, \\ t_0 \sum_{j=1}^4 \beta_j \phi_A^{(j)} + t_b^+ \sum_{j=1}^4 \beta_j^2 \phi_B^{(j)} - V \sum_{j=1}^4 \beta_j \phi_B^{(j)} = E_{\text{OBC}} \sum_{j=1}^4 \beta_j \phi_B^{(j)}, \\ t_a^- \sum_{j=1}^4 \beta_j^{L-1} \phi_A^{(j)} + t_0 \sum_{j=1}^4 \beta_j^L \phi_B^{(j)} + V \sum_{j=1}^4 \beta_j^L \phi_A^{(j)} = E_{\text{OBC}} \sum_{j=1}^4 \beta_j^L \phi_A^{(j)}, \\ t_b^- \sum_{j=1}^4 \beta_j^{L-1} \phi_B^{(j)} + t_0 \sum_{j=1}^4 \beta_j^L \phi_A^{(j)} - V \sum_{j=1}^4 \beta_j^L \phi_B^{(j)} = E_{\text{OBC}} \sum_{j=1}^4 \beta_j^L \phi_B^{(j)}, \end{cases} \quad (\text{D2})$$

Furthermore, by using the bulk eigenequation in Eq. (22):

$$\begin{cases} (t_a^+ \beta + t_a^- \beta^{-1} + V - E_{\text{OBC}}) \phi_A + t_0 \phi_B = 0, & \frac{\phi_B}{\phi_A} = -\frac{(t_a^+ \beta + t_a^- \beta^{-1} + V - E_{\text{OBC}}) t_0}{t_0}, \\ t_0 \phi_A + (t_b^+ \beta + t_b^- \beta^{-1} - V - E_{\text{OBC}}) \phi_B = 0, & \frac{\phi_B}{\phi_A} = -\frac{t_0}{(t_b^+ \beta + t_b^- \beta^{-1} - V - E_{\text{OBC}})}, \end{cases} \quad (\text{D3})$$

i.e.,

$$\frac{\phi_B^{(j)}}{\phi_A^{(j)}} = \frac{(E_{\text{OBC}} - t_a^+ \beta_j - t_a^- \beta_j^{-1} - V)}{t_0} = \frac{t_0}{(E_{\text{OBC}} - t_b^+ \beta_j - t_b^- \beta_j^{-1} + V)} = f_j, \quad (\text{D4})$$

$$t_0^2 = (E_{\text{OBC}} - t_a^+ \beta_j - t_a^- \beta_j^{-1} - V)(E_{\text{OBC}} - t_b^+ \beta_j - t_b^- \beta_j^{-1} + V), \quad (\text{D5})$$

$$\phi_B^{(j)} = f_j \phi_A^{(j)}, \quad (\text{D6})$$

we have

$$\begin{cases} t_0 \sum_{j=1}^4 \beta_j f_j \phi_A^{(j)} + t_a^+ \sum_{j=1}^4 \beta_j^2 \phi_A^{(j)} + V \sum_{j=1}^4 \beta_j \phi_A^{(j)} = E_{\text{OBC}} \sum_{j=1}^4 \beta_j \phi_A^{(j)}, \\ t_0 \sum_{j=1}^4 \beta_j \phi_A^{(j)} + t_b^+ \sum_{j=1}^4 \beta_j^2 f_j \phi_A^{(j)} - V \sum_{j=1}^4 \beta_j f_j \phi_A^{(j)} = E_{\text{OBC}} \sum_{j=1}^4 \beta_j f_j \phi_A^{(j)}, \\ t_a^- \sum_{j=1}^4 \beta_j^{L-1} \phi_A^{(j)} + t_0 \sum_{j=1}^4 \beta_j^L f_j \phi_A^{(j)} + V \sum_{j=1}^4 \beta_j^L \phi_A^{(j)} = E_{\text{OBC}} \sum_{j=1}^4 \beta_j^L \phi_A^{(j)}, \\ t_b^- \sum_{j=1}^4 \beta_j^{L-1} f_j \phi_A^{(j)} + t_0 \sum_{j=1}^4 \beta_j^L \phi_A^{(j)} - V \sum_{j=1}^4 \beta_j^L f_j \phi_A^{(j)} = E_{\text{OBC}} \sum_{j=1}^4 \beta_j^L f_j \phi_A^{(j)}, \end{cases} \quad (\text{D7})$$

$$\begin{cases} \sum_{j=1}^4 (E_{\text{OBC}} - t_a^+ \beta_j - t_a^- \beta_j^{-1} - V) \beta_j \phi_A^{(j)} + t_a^+ \sum_{j=1}^4 \beta_j^2 \phi_A^{(j)} + V \sum_{j=1}^4 \beta_j \phi_A^{(j)} = E_{\text{OBC}} \sum_{j=1}^4 \beta_j \phi_A^{(j)}, \\ t_0 \sum_{j=1}^4 \beta_j \phi_A^{(j)} + \sum_{j=1}^4 (t_b^+ \beta_j - V - E_{\text{OBC}}) \beta_j f_j \phi_A^{(j)} = 0, \\ t_a^- \sum_{j=1}^4 \beta_j^{L-1} \phi_A^{(j)} + \sum_{j=1}^4 (E_{\text{OBC}} - t_a^+ \beta_j - t_a^- \beta_j^{-1} - V) \beta_j^L \phi_A^{(j)} + V \sum_{j=1}^4 \beta_j^L \phi_A^{(j)} = E_{\text{OBC}} \sum_{j=1}^4 \beta_j^L \phi_A^{(j)}, \\ \sum_{j=1}^4 (t_b^- \beta_j^{L-1} - V - E_{\text{OBC}}) \beta_j^L f_j \phi_A^{(j)} + t_0 \sum_{j=1}^4 \beta_j^L \phi_A^{(j)} = 0, \end{cases} \quad (\text{D8})$$

$$\begin{cases} \sum_{j=1}^4 (-t_a^- \beta_j^{-1}) \beta_j \phi_A^{(j)} = 0, \\ \sum_{j=1}^4 \beta_j \phi_A^{(j)} + \sum_{j=1}^4 \frac{(t_b^+ \beta_j - V - E_{\text{OBC}})}{(E_{\text{OBC}} - t_b^+ \beta_j - t_b^- \beta_j^{-1} + V)} \beta_j \phi_A^{(j)} = 0, \\ \sum_{j=1}^4 (-t_a^+ \beta_j) \beta_j^L \phi_A^{(j)} = 0, \\ \sum_{j=1}^4 \frac{(t_b^- \beta_j^{L-1} - V - E_{\text{OBC}})}{(E_{\text{OBC}} - t_b^+ \beta_j - t_b^- \beta_j^{-1} + V)} \beta_j^L \phi_A^{(j)} + \sum_{j=1}^4 \beta_j^L \phi_A^{(j)} = 0, \end{cases} \quad (\text{D9})$$

$$\begin{cases} \sum_{j=1}^4 \phi_A^{(j)} = 0, \\ \sum_{j=1}^4 \frac{1}{(E_{\text{OBC}} - t_b^+ \beta_j - t_b^- \beta_j^{-1} + V)} \phi_A^{(j)} = 0, \quad \sum_{j=1}^4 \phi_A^{(j)} = \sum_{j=1}^4 (E_{\text{OBC}} - t_a^+ \beta_j - t_a^- \beta_j^{-1} - V) \phi_A^{(j)} = 0, \\ \sum_{j=1}^4 \beta_j^{L+1} \phi_A^{(j)} = 0, \\ \sum_{j=1}^4 \frac{1}{(E_{\text{OBC}} - t_b^+ \beta_j - t_b^- \beta_j^{-1} + V)} \beta_j^{L+1} \phi_A^{(j)} = 0, \quad \sum_{j=1}^4 (E_{\text{OBC}} - t_a^+ \beta_j - t_a^- \beta_j^{-1} - V) \beta_j^{L+1} \phi_A^{(j)} = 0, \end{cases} \quad (\text{D10})$$

where we have used the characteristic dispersion equation

$$\frac{1}{(E_{\text{OBC}} - t_b^+ \beta_j - t_b^- \beta_j^{-1} + V)} = \frac{(E_{\text{OBC}} - t_a^+ \beta_j - t_a^- \beta_j^{-1} - V)}{t_0^2}. \quad (\text{D11})$$

Imposing the condition that  $\phi_A^{(j)}$  ( $j = 1, 2, 3, 4$ ) do not vanish, we must have the vanishing determinant:

$$\begin{vmatrix} 1 & 1 & 1 & 1 \\ X_1 & X_2 & X_3 & X_4 \\ \beta_1^{L+1} & \beta_2^{L+1} & \beta_3^{L+1} & \beta_4^{L+1} \\ X_1 \beta_1^{L+1} & X_2 \beta_2^{L+1} & X_3 \beta_3^{L+1} & X_4 \beta_4^{L+1} \end{vmatrix} = 0, \quad (\text{D12})$$

where  $|\beta_1| \leq |\beta_2| \leq |\beta_3| \leq |\beta_4|$ . Here,  $X_j$  ( $j = 1, 2, 3, 4$ ) are defined as

$$X_j \equiv E_{\text{OBC}} - t_a^+ \beta_j - t_a^- \beta_j^{-1} - V, \quad (j = 1, 2, 3, 4). \quad (\text{D13})$$

Simplifying, we obtain the boundary equation (24) from Eq. (D12):

$$X_{1,4} X_{2,3} \left[ (\beta_1 \beta_4)^{L+1} + (\beta_2 \beta_3)^{L+1} \right] - X_{1,3} X_{2,4} \left[ (\beta_1 \beta_3)^{L+1} + (\beta_2 \beta_4)^{L+1} \right] + X_{1,2} X_{3,4} \left[ (\beta_1 \beta_2)^{L+1} + (\beta_3 \beta_4)^{L+1} \right] = 0, \quad (\text{D14})$$

where  $X_{i,j}$  ( $i, j = 1, 2, 3, 4$ ) are defined as

$$X_{i,j} \equiv X_i - X_j = t_a^+ (\beta_j - \beta_i) + t_a^- (\beta_j^{-1} - \beta_i^{-1}), \quad (i, j = 1, 2, 3, 4). \quad (\text{D15})$$

### Appendix E: Derivation of Eq. (26)

We start from the characteristic equation of our coupled Hatano-Nelson model with offset:

$$\begin{aligned} & t_a^+ t_b^+ \beta^2 + [-(t_a^+ + t_b^+) E_{\text{OBC}} - (t_a^+ - t_b^+) V] \beta + (t_a^+ t_b^- + t_a^- t_b^+ + E_{\text{OBC}}^2 - t_0^2 - V^2) \\ & + [-(t_a^- + t_b^-) E_{\text{OBC}} - (t_a^- - t_b^-) V] \beta^{-1} + t_a^- t_b^- \beta^{-2} = 0. \end{aligned} \quad (\text{E1})$$

We consider a perturbative solution up to the second order in  $t_0$  by first expanding in terms of the  $\beta$ s:

$$\begin{cases} \beta_1 \simeq x_-^{(a)} + y_-^{(a)} t_0^2, \\ \beta_2 \simeq x_+^{(a)} + y_+^{(a)} t_0^2, \\ \beta_3 \simeq x_-^{(b)} + y_-^{(b)} t_0^2, \\ \beta_4 \simeq x_+^{(b)} + y_+^{(b)} t_0^2, \end{cases} \quad (\text{E2})$$

where  $t_a^+ > t_a^-$ ,  $t_b^+ < t_b^-$ ,  $t_a^+ > t_b^+$ ,  $V > 0$ ,  $|\beta_1| \leq |\beta_2| \leq |\beta_3| \leq |\beta_4|$ ,

$$\begin{cases} x_{\pm}^{(a)} = \frac{1}{2t_a^+} (E_{\text{OBC}} - V \pm \Delta_a), \\ x_{\pm}^{(b)} = \frac{1}{2t_b^+} (E_{\text{OBC}} + V \pm \Delta_b), \\ y_{\pm}^{(a)} = \frac{-[E_{\text{OBC}}^2 - 2t_a^+ t_a^- + V(V \mp \Delta_a) - (2V \mp \Delta_a) E_{\text{OBC}}]}{g_{\pm}^{(a)}}, \\ y_{\pm}^{(b)} = \frac{[E_{\text{OBC}}^2 - 2t_b^+ t_b^- + V(V \pm \Delta_b) + (2V \pm \Delta_b) E_{\text{OBC}}]}{g_{\pm}^{(b)}}, \end{cases} \quad (\text{E3})$$



and

$$\Delta_a = \sqrt{(E_{\text{OBC}} - V)^2 - 4t_a^+ t_a^-}, \quad (\text{E4})$$

$$\Delta_b = \sqrt{(E_{\text{OBC}} + V)^2 - 4t_b^+ t_b^-}, \quad (\text{E5})$$

$$\begin{aligned} g_{\pm}^{(a)} = & E_{\text{OBC}}^3(t_a^+ - t_b^+) - 4t_a^+ t_a^-(t_a^+ + t_b^+)V + (t_a^+ + t_b^+)V^3 \mp 2t_a^+(t_a^+ t_b^- - t_a^- t_b^+)\Delta_a \\ & \mp (t_a^+ + t_b^+)\Delta_a V^2 + E_{\text{OBC}}^2[(3t_b^+ - t_a^+)V \pm (t_a^+ - t_b^+)\Delta_a] \\ & + E_{\text{OBC}}[-4t_a^+ t_a^-(t_a^+ - t_b^+) - (t_a^+ + 3t_b^+)V^2 \pm 2t_b^+\Delta_a V], \end{aligned} \quad (\text{E6})$$

$$\begin{aligned} g_{\pm}^{(b)} = & E_{\text{OBC}}^3(t_a^+ - t_b^+) - 4t_b^+ t_b^-(t_a^+ + t_b^+)V + (t_a^+ + t_b^+)V^3 \mp 2t_b^+(t_a^+ t_b^- - t_a^- t_b^+)\Delta_b \\ & \pm (t_a^+ + t_b^+)\Delta_b V^2 + E_{\text{OBC}}^2[(3t_a^+ - t_b^+)V \pm (t_a^+ - t_b^+)\Delta_b] \\ & + E_{\text{OBC}}[-4t_b^+ t_b^-(t_a^+ - t_b^+) + (t_b^+ + 3t_a^+)V^2 \pm 2t_a^+\Delta_b V]. \end{aligned} \quad (\text{E7})$$

With Eq. (E2) and (D13), we can get

$$\begin{cases} X_{1,2} = \frac{(t_a^+ t_b^- - t_a^- t_b^+)\Delta_a t_0^2}{E_{\text{OBC}}^2(t_a^- - t_b^-)(t_a^+ - t_b^+) + (t_a^+ t_b^- - t_a^- t_b^+)^2 + 2E_{\text{OBC}}V(t_a^+ t_a^- - t_b^+ t_b^-) + (t_a^- + t_b^-)(t_a^+ + t_b^+)V^2} + \mathcal{O}(t_0^4), \\ X_{3,4} = \left(\frac{t_a^+}{t_b^+} - \frac{t_a^-}{t_b^-}\right)\Delta_b + \mathcal{O}(t_0^2), \\ X_{1,3} = \frac{1}{2} \left[ \frac{t_a^+}{t_b^+} (E_{\text{OBC}} + V - \Delta_b) - (E_{\text{OBC}} - V - \Delta_a) \right] + \left[ \frac{2t_b^+ t_a^-}{E_{\text{OBC}} + V - \Delta_b} - \frac{2t_a^+ t_a^-}{E_{\text{OBC}} - V - \Delta_a} \right] + \mathcal{O}(t_0^2), \\ X_{2,4} = \frac{1}{2} \left[ \frac{t_a^+}{t_b^+} (E_{\text{OBC}} + V + \Delta_b) - (E_{\text{OBC}} - V + \Delta_a) \right] + \left[ \frac{2t_b^+ t_a^-}{E_{\text{OBC}} + V + \Delta_b} - \frac{2t_a^+ t_a^-}{E_{\text{OBC}} - V + \Delta_a} \right] + \mathcal{O}(t_0^2). \end{cases} \quad (\text{E8})$$

We can obtain Eq. (26) by substituting Eq. (E8) into  $X_{1,2}X_{3,4}/(X_{1,3}X_{2,4})$  and expanding up to the second order in  $t_0$ .

## Appendix F: OBC spectra for topologically coupled chain model

In this appendix, in order to understand why the topological zero modes appear at  $E = 0$  in the point gap only at sufficiently large system sizes, we show the OBC energy spectra of the topologically coupled chain model (33) with  $V = 0$  for various system sizes.

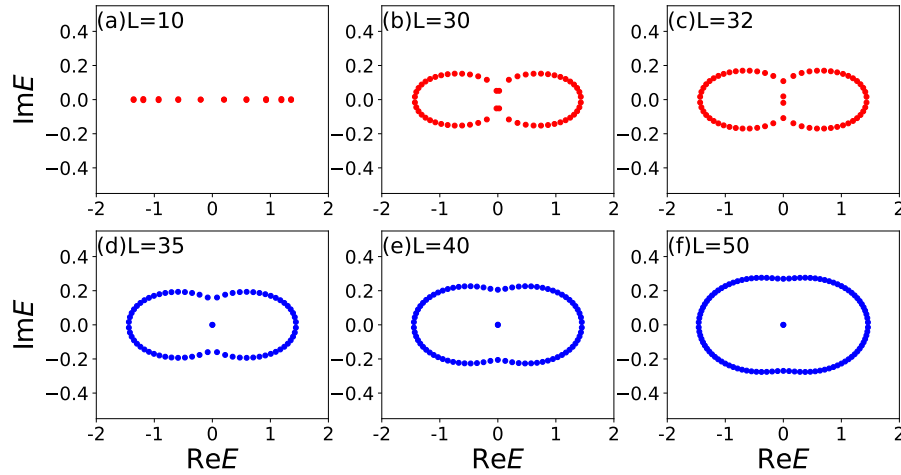


FIG. 13. OBC energy spectra of the topologically coupled chain model Hamiltonian (33) with  $V = 0$  at different system sizes (a)  $L = 10$ , (b)  $L = 30$ , (c)  $L = 32$ , (d)  $L = 35$ , (e)  $L = 40$ , (f)  $L = 50$ . Notably, topological zero modes appear at  $E = 0$  in the point gap only at sufficiently large system sizes of  $L = 35, 40, 50$ . The other parameters are  $\delta_{ab} = 0.5 \times 10^{-3}$ ,  $t_1 = 0.75$ , and  $\delta_a = -\delta_b = 0.25$ .

It is indicated from Fig. 13 that, when we tune the system size  $L$  (regarding  $L$  as a parameter), the OBC spectrum changes. At a critical  $L$ , the OBC spectrum's gap closes and after that, topological zero modes appear.

### Appendix G: Derivation of Eq. (35)

In this appendix, we describe the derivation of Eq. (35), which expresses the OBC constraint of our coupled topological model. Under OBCs, we can write the real-space Schrödinger equation  $\mathcal{H}_t|\psi\rangle = E_{\text{OBC}}|\psi\rangle$  [where  $\mathcal{H}_t$  is the Hamiltonian matrix of  $H_t$  in the basis  $(C_1, C_2, \dots, C_L)^T$ ], where  $|\psi\rangle = (\psi_{1,A}, \psi_{1,B}, \psi_{2,A}, \psi_{2,B}, \dots, \psi_{n,A}, \psi_{n,B}, \dots)^T$ , as

$$\begin{cases} t_a^- \psi_{n-1,A} + \delta_{ab} \psi_{n-1,B} + V \psi_{n,A} + t_a^+ \psi_{n+1,A} + \delta_{ab} \psi_{n+1,B} = E_{\text{OBC}} \psi_{n,A}, \\ t_b^- \psi_{n-1,B} - \delta_{ab} \psi_{n-1,A} - V \psi_{n,B} + t_b^+ \psi_{n+1,B} - \delta_{ab} \psi_{n+1,A} = E_{\text{OBC}} \psi_{n,B}. \end{cases} \quad (\text{G1})$$

According to the theory of linear difference equations, we can take as an ansatz for the eigenstates the linear combination:

$$\begin{pmatrix} \psi_{n,A} \\ \psi_{n,B} \end{pmatrix} = \sum_{j=1}^4 \beta_j^n \begin{pmatrix} \phi_A^{(j)} \\ \phi_B^{(j)} \end{pmatrix}. \quad (\text{G2})$$

Hence, Eq. (G1) can be rewritten as

$$\begin{pmatrix} t_a^+ \beta + t_a^- \beta^{-1} + V & \delta_{ab}(\beta + \beta^{-1}) \\ -\delta_{ab}(\beta + \beta^{-1}) & t_b^+ \beta + t_b^- \beta^{-1} - V \end{pmatrix} \begin{pmatrix} \phi_A \\ \phi_B \end{pmatrix} = E_{\text{OBC}} \begin{pmatrix} \phi_A \\ \phi_B \end{pmatrix}. \quad (\text{G3})$$

From the real-space eigenequation in Eq. (G1) and the open boundary conditions  $\psi_{0,\alpha} = \psi_{L+1,\alpha} = 0$  ( $\alpha = A, B$ ), we can get the equations for the eigenstates in real space as

$$\begin{cases} \delta_{ab} \psi_{2,B} + t_a^+ \psi_{2,A} + V \psi_{1,A} = E_{\text{OBC}} \psi_{1,A}, \\ -\delta_{ab} \psi_{2,A} + t_b^+ \psi_{2,B} - V \psi_{1,B} = E_{\text{OBC}} \psi_{1,B}, \\ t_a^- \psi_{L-1,A} + \delta_{ab} \psi_{L-1,B} + V \psi_{L,A} = E_{\text{OBC}} \psi_{L,A}, \\ t_b^- \psi_{L-1,B} - \delta_{ab} \psi_{L-1,A} - V \psi_{L,B} = E_{\text{OBC}} \psi_{L,B}. \end{cases} \quad (\text{G4})$$

Now, Eq. (G4) can be rewritten into coupled equations for the coefficients  $\phi_\alpha^{(j)}$  ( $\alpha = A, B$ ;  $j = 1, 2, 3, 4$ ) by substituting the general solution  $(\psi_{n,A}, \psi_{n,B})^T = \sum_{j=1}^4 \beta_j^n (\phi_A^{(j)}, \phi_B^{(j)})^T$  as

$$\begin{cases} \delta_{ab} \sum_{j=1}^4 \beta_j^2 \phi_B^{(j)} + t_a^+ \sum_{j=1}^4 \beta_j^2 \phi_A^{(j)} + V \sum_{j=1}^4 \beta_j \phi_A^{(j)} = E_{\text{OBC}} \sum_{j=1}^4 \beta_j \phi_A^{(j)}, \\ -\delta_{ab} \sum_{j=1}^4 \beta_j^2 \phi_A^{(j)} + t_b^+ \sum_{j=1}^4 \beta_j^2 \phi_B^{(j)} - V \sum_{j=1}^4 \beta_j \phi_B^{(j)} = E_{\text{OBC}} \sum_{j=1}^4 \beta_j \phi_B^{(j)}, \\ t_a^- \sum_{j=1}^4 \beta_j^{L-1} \phi_A^{(j)} + \delta_{ab} \sum_{j=1}^4 \beta_j^{L-1} \phi_B^{(j)} + V \sum_{j=1}^4 \beta_j^L \phi_A^{(j)} = E_{\text{OBC}} \sum_{j=1}^4 \beta_j^L \phi_A^{(j)}, \\ t_b^- \sum_{j=1}^4 \beta_j^{L-1} \phi_B^{(j)} - \delta_{ab} \sum_{j=1}^4 \beta_j^{L-1} \phi_A^{(j)} - V \sum_{j=1}^4 \beta_j^L \phi_B^{(j)} = E_{\text{OBC}} \sum_{j=1}^4 \beta_j^L \phi_B^{(j)}. \end{cases} \quad (\text{G5})$$

Furthermore, by using the bulk eigenequation in Eq. (G3):

$$\begin{cases} (t_a^+ \beta + t_a^- \beta^{-1} + V - E_{\text{OBC}}) \phi_A + \delta_{ab}(\beta + \beta^{-1}) \phi_B = 0, & \frac{\phi_B}{\phi_A} = -\frac{(t_a^+ \beta + t_a^- \beta^{-1} + V - E_{\text{OBC}})}{\delta_{ab}(\beta + \beta^{-1})}, \\ -\delta_{ab}(\beta + \beta^{-1}) \phi_A + (t_b^+ \beta + t_b^- \beta^{-1} - V - E_{\text{OBC}}) \phi_B = 0, & \frac{\phi_B}{\phi_A} = \frac{\delta_{ab}(\beta + \beta^{-1})}{(t_b^+ \beta + t_b^- \beta^{-1} - V - E_{\text{OBC}})}, \end{cases} \quad (\text{G6})$$

i.e.,

$$\frac{\phi_B^{(j)}}{\phi_A^{(j)}} = \frac{(E_{\text{OBC}} - t_a^+ \beta_j - t_a^- \beta_j^{-1} - V)}{\delta_{ab}(\beta + \beta^{-1})} = \frac{-\delta_{ab}(\beta + \beta^{-1})}{(E_{\text{OBC}} - t_b^+ \beta_j - t_b^- \beta_j^{-1} + V)} = f_j, \quad (\text{G7})$$

$$-\delta_{ab}^2(\beta + \beta^{-1})^2 = (E_{\text{OBC}} - t_a^+ \beta_j - t_a^- \beta_j^{-1} - V)(E_{\text{OBC}} - t_b^+ \beta_j - t_b^- \beta_j^{-1} + V), \quad (\text{G8})$$

$$\phi_B^{(j)} = f_j \phi_A^{(j)}. \quad (\text{G9})$$

The general solution is written as a linear combination:

$$\begin{pmatrix} \psi_{n,A} \\ \psi_{n,B} \end{pmatrix} = \beta_1^n \begin{pmatrix} \phi_A^{(1)} \\ \phi_B^{(1)} \end{pmatrix} + \beta_2^n \begin{pmatrix} \phi_A^{(2)} \\ \phi_B^{(2)} \end{pmatrix} + \beta_3^n \begin{pmatrix} \phi_A^{(3)} \\ \phi_B^{(3)} \end{pmatrix} + \beta_4^n \begin{pmatrix} \phi_A^{(4)} \\ \phi_B^{(4)} \end{pmatrix} \quad (\text{G10})$$

which should satisfy the open boundary conditions (G5):

$$\begin{cases} \delta_{ab} \sum_{j=1}^4 \beta_j^2 f_j \phi_A^{(j)} + t_a^+ \sum_{j=1}^4 \beta_j^2 \phi_A^{(j)} + V \sum_{j=1}^4 \beta_j \phi_A^{(j)} = E_{\text{OBC}} \sum_{j=1}^4 \beta_j \phi_A^{(j)}, \\ -\delta_{ab} \sum_{j=1}^4 \beta_j^2 \phi_A^{(j)} + t_b^+ \sum_{j=1}^4 \beta_j^2 f_j \phi_A^{(j)} - V \sum_{j=1}^4 \beta_j f_j \phi_A^{(j)} = E_{\text{OBC}} \sum_{j=1}^4 \beta_j f_j \phi_A^{(j)}, \\ t_a^- \sum_{j=1}^4 \beta_j^{L-1} \phi_A^{(j)} + \delta_{ab} \sum_{j=1}^4 \beta_j^{L-1} f_j \phi_A^{(j)} + V \sum_{j=1}^4 \beta_j^L \phi_A^{(j)} = E_{\text{OBC}} \sum_{j=1}^4 \beta_j^L \phi_A^{(j)}, \\ t_b^- \sum_{j=1}^4 \beta_j^{L-1} f_j \phi_A^{(j)} - \delta_{ab} \sum_{j=1}^4 \beta_j^{L-1} \phi_A^{(j)} - V \sum_{j=1}^4 \beta_j^L f_j \phi_A^{(j)} = E_{\text{OBC}} \sum_{j=1}^4 \beta_j^L f_j \phi_A^{(j)}, \end{cases} \quad (\text{G11})$$

$$\begin{cases} \sum_{j=1}^4 \frac{(E_{\text{OBC}} - t_a^+ \beta_j - t_a^- \beta_j^{-1} - V)}{\beta_j + \beta_j^{-1}} \beta_j^2 \phi_A^{(j)} = \sum_{j=1}^4 (E_{\text{OBC}} - t_a^+ \beta_j - V) \beta_j \phi_A^{(j)}, \\ -\delta_{ab} \sum_{j=1}^4 \beta_j^2 \phi_A^{(j)} + \sum_{j=1}^4 (t_b^+ \beta_j - V - E_{\text{OBC}}) \beta_j f_j \phi_A^{(j)} = 0, \\ \sum_{j=1}^4 \frac{(E_{\text{OBC}} - t_a^+ \beta_j - t_a^- \beta_j^{-1} - V)}{\beta_j + \beta_j^{-1}} \beta_j^{L-1} \phi_A^{(j)} = \sum_{j=1}^4 (E_{\text{OBC}} - t_a^- \beta_j^{-1} - V) \beta_j^L \phi_A^{(j)}, \\ \sum_{j=1}^4 (t_b^- \beta_j^{-1} - V - E_{\text{OBC}}) \beta_j^L f_j \phi_A^{(j)} - \delta_{ab} \sum_{j=1}^4 \beta_j^{L-1} \phi_A^{(j)} = 0, \end{cases} \quad (\text{G12})$$

$$\begin{cases} \sum_{j=1}^4 [(E_{\text{OBC}} - t_a^+ \beta_j - t_a^- \beta_j^{-1} - V) \beta_j - (E_{\text{OBC}} - t_a^+ \beta_j - V)(\beta_j + \beta_j^{-1})] \beta_j \phi_A^{(j)} = 0, \\ \sum_{j=1}^4 \beta_j^2 \phi_A^{(j)} + \sum_{j=1}^4 \frac{(\beta_j + \beta_j^{-1})(t_b^+ \beta_j - V - E_{\text{OBC}})}{(E_{\text{OBC}} - t_b^+ \beta_j - t_b^- \beta_j^{-1} + V)} \beta_j \phi_A^{(j)} = 0, \\ \sum_{j=1}^4 [(E_{\text{OBC}} - t_a^+ \beta_j - t_a^- \beta_j^{-1} - V) \beta_j^{-1} - (E_{\text{OBC}} - t_a^- \beta_j^{-1} - V)(\beta_j + \beta_j^{-1})] \beta_j^L \phi_A^{(j)} = 0, \\ \sum_{j=1}^4 \frac{(\beta_j + \beta_j^{-1})(t_b^- \beta_j^{-1} - V - E_{\text{OBC}})}{(E_{\text{OBC}} - t_b^+ \beta_j - t_b^- \beta_j^{-1} + V)} \beta_j^L \phi_A^{(j)} + \sum_{j=1}^4 \beta_j^{L-1} \phi_A^{(j)} = 0, \end{cases} \quad (\text{G13})$$

$$\begin{cases} \sum_{j=1}^4 [-t_a^- - (E_{\text{OBC}} - t_a^+ \beta_j - V) \beta_j^{-1}] \beta_j \phi_A^{(j)} = 0, \\ \sum_{j=1}^4 [(E_{\text{OBC}} - t_b^+ \beta_j - t_b^- \beta_j^{-1} + V) \beta_j - (E_{\text{OBC}} - t_b^+ \beta_j + V)(\beta_j + \beta_j^{-1})] \beta_j \phi_A^{(j)} = 0, \\ \sum_{j=1}^4 [-t_a^+ - (E_{\text{OBC}} - t_a^- \beta_j^{-1} - V) \beta_j] \beta_j^L \phi_A^{(j)} = 0, \\ \sum_{j=1}^4 [(E_{\text{OBC}} - t_b^+ \beta_j - t_b^- \beta_j^{-1} + V) \beta_j^{-1} - (E_{\text{OBC}} - t_b^- \beta_j^{-1} + V)(\beta_j + \beta_j^{-1})] \beta_j^L \phi_A^{(j)} = 0, \end{cases} \quad (\text{G14})$$

$$\begin{cases} \sum_{j=1}^4 [-t_a^- - (E_{\text{OBC}} - t_a^+ \beta_j - V) \beta_j^{-1}] \beta_j \phi_A^{(j)} = 0, \\ \sum_{j=1}^4 [-t_b^- - (E_{\text{OBC}} - t_b^+ \beta_j + V) \beta_j^{-1}] \beta_j \phi_A^{(j)} = 0, \\ \sum_{j=1}^4 [-t_a^+ - (E_{\text{OBC}} - t_a^- \beta_j^{-1} - V) \beta_j] \beta_j^L \phi_A^{(j)} = 0, \\ \sum_{j=1}^4 [-t_b^+ - (E_{\text{OBC}} - t_b^- \beta_j^{-1} + V) \beta_j] \beta_j^L \phi_A^{(j)} = 0, \end{cases} \quad (\text{G15})$$

$$\begin{cases} \sum_{j=1}^4 [E_{\text{OBC}} - (t_a^+ - t_a^-) \beta_j - V] \phi_A^{(j)} = 0, \\ \sum_{j=1}^4 [E_{\text{OBC}} - (t_b^+ - t_b^-) \beta_j + V] \phi_A^{(j)} = 0, \\ \sum_{j=1}^4 [E_{\text{OBC}} + (t_a^+ - t_a^-) \beta_j^{-1} - V] \beta_j^{L+1} \phi_A^{(j)} = 0, \\ \sum_{j=1}^4 [E_{\text{OBC}} + (t_b^+ - t_b^-) \beta_j^{-1} + V] \beta_j^{L+1} \phi_A^{(j)} = 0. \end{cases} \quad (\text{G16})$$

Here, we have obtained the coupled equations in terms of only  $\phi_A^{(j)}$  ( $j = 1, 2, 3, 4$ ). For  $\phi_A^{(j)}$  ( $j = 1, 2, 3, 4$ ) to have nonzero values, the determinant condition is

$$\begin{vmatrix} X_1^{(a)} & X_2^{(a)} & X_3^{(a)} & X_4^{(a)} \\ Y_1^{(a)} & Y_2^{(a)} & Y_3^{(a)} & Y_4^{(a)} \\ X_1^{(b)}\beta_1^{L+1} & X_2^{(b)}\beta_2^{L+1} & X_3^{(b)}\beta_3^{L+1} & X_4^{(b)}\beta_4^{L+1} \\ Y_1^{(b)}\beta_1^{L+1} & Y_2^{(b)}\beta_2^{L+1} & Y_3^{(b)}\beta_3^{L+1} & Y_4^{(b)}\beta_4^{L+1} \end{vmatrix} = 0 \quad (\text{G17})$$

with  $|\beta_1| \leq |\beta_2| \leq |\beta_3| \leq |\beta_4|$ . Here,  $X_j$  and  $Y_j$  ( $j = 1, \dots, 4$ ) are defined as

$$X_j^{(a)} = E_{\text{OBC}} - (t_a^+ - t_a^-)\beta_j - V = E_{\text{OBC}} - 2\delta_a\beta_j - V, \quad (j = 1, \dots, 4), \quad (\text{G18})$$

$$Y_j^{(a)} = E_{\text{OBC}} - (t_b^+ - t_b^-)\beta_j + V = E_{\text{OBC}} - 2\delta_b\beta_j + V, \quad (j = 1, \dots, 4), \quad (\text{G19})$$

$$X_j^{(b)} = E_{\text{OBC}} + (t_a^+ - t_a^-)\beta_j^{-1} - V = E_{\text{OBC}} + 2\delta_a\beta_j^{-1} - V, \quad (j = 1, \dots, 4), \quad (\text{G20})$$

$$Y_j^{(b)} = E_{\text{OBC}} + (t_b^+ - t_b^-)\beta_j^{-1} + V = E_{\text{OBC}} + 2\delta_b\beta_j^{-1} + V, \quad (j = 1, \dots, 4). \quad (\text{G21})$$

Finally, we can obtain the boundary equation (35) from Eq. (G17) as

$$\begin{aligned} & \left[ Z_{1,4}^{(b)} Z_{2,3}^{(a)} (\beta_1 \beta_4)^{L+1} + Z_{1,4}^{(a)} Z_{2,3}^{(b)} (\beta_2 \beta_3)^{L+1} \right] \\ & - \left[ Z_{1,3}^{(b)} Z_{2,4}^{(a)} (\beta_1 \beta_3)^{L+1} + Z_{1,3}^{(a)} Z_{2,4}^{(b)} (\beta_2 \beta_4)^{L+1} \right] \\ & + \left[ Z_{1,2}^{(b)} Z_{3,4}^{(a)} (\beta_1 \beta_2)^{L+1} + Z_{1,2}^{(a)} Z_{3,4}^{(b)} (\beta_3 \beta_4)^{L+1} \right] = 0, \end{aligned} \quad (\text{G22})$$

where  $\beta_j$  ( $j = 1, 2, 3, 4$ ) satisfy  $|\beta_1| \leq |\beta_2| \leq |\beta_3| \leq |\beta_4|$ , and  $Z_{i,j}^{(c)}$  ( $i, j = 1, 2, 3, 4$ ;  $c = a, b$ ) are defined as

$$Z_{i,j}^{(c)} = X_i^{(c)} Y_j^{(c)} - X_j^{(c)} Y_i^{(c)} \quad (\text{G23})$$

$$= \begin{cases} [(t_b^+ - t_b^-)(E_{\text{OBC}} - V) - (t_a^+ - t_a^-)(E_{\text{OBC}} + V)](\beta_i - \beta_j), & c = a \\ [(t_b^+ - t_b^-)(E_{\text{OBC}} - V) - (t_a^+ - t_a^-)(E_{\text{OBC}} + V)](\beta_j^{-1} - \beta_i^{-1}), & c = b \end{cases}, \quad (\text{G24})$$

where  $i, j = 1, 2, 3, 4$ ;  $c = a, b$ .